nature biotechnology

ARTICLES

https://doi.org/10.1038/s41587-020-00763-w



# Generation of human striatal organoids and cortico-striatal assembloids from human pluripotent stem cells

Yuki Miura[1,2], Min-Yin Li[1,2], Fikri Birey[1,2], Kazuya Ikeda[3], Omer Revah[1,2], Mayuri Vijay Thete[1,2], Jin-Young Park[1,2], Alyssa Puno[3], Samuel H. Lee[1], Matthew H. Porteus[3] and Sergiu P. Pașca[1,2]✉

**Cortico-striatal projections are critical components of forebrain circuitry that regulate motivated behaviors. To enable the study of the human cortico-striatal pathway and how its dysfunction leads to neuropsychiatric disease, we developed a method to convert human pluripotent stem cells into region-specific brain organoids that resemble the developing human striatum and include electrically active medium spiny neurons. We then assembled these organoids with cerebral cortical organoids in three-dimensional cultures to form cortico-striatal assembloids. Using viral tracing and functional assays in intact or sliced assembloids, we show that cortical neurons send axonal projections into striatal organoids and form synaptic connections. Medium spiny neurons mature electrophysiologically following assembly and display calcium activity after optogenetic stimulation of cortical neurons. Moreover, we derive cortico-striatal assembloids from patients with a neurodevelopmental disorder caused by a deletion on chromosome 22q13.3 and capture disease-associated defects in calcium activity, showing that this approach will allow investigation of the development and functional assembly of cortico-striatal connectivity using patient-derived cells.**

Neural activity in cortico-striatal circuits of the forebrain coordinates motivated behaviors and movement[1,2]. In this pathway, glutamatergic neurons in the cerebral cortex project to the striatum, where they connect primarily to GABAergic medium spiny neurons that subsequently connect to downstream circuits in the basal ganglia (Fig. 1a). Dysfunctions in neural circuits of the cortico-striatal pathway are thought to contribute to neurodevelopmental disorders, such as autism spectrum disorder (ASD), schizophrenia and obsessive–compulsive disorder[2–5]. However, how these circuits are assembled during human development and how functional defects arise in disease in human patients is still poorly understood. Therefore, new in vitro approaches to image and functionally manipulate human cortico-striatal circuits will facilitate research on their roles in neuropsychiatric disorders[6].

Human pluripotent stem (hPS) cells, including human induced pluripotent stem (hiPS) cells, have the ability to differentiate into any of the germ layers and, with the advent of three-dimensional (3D) culture methods[7], to self-organize in brain organoids[8] and generate diverse cell types in the central nervous system[9–13]. These cultures can, in principle, be derived from any individual and can be employed to study cell specification, model cell–cell interactions[14] and investigate disease[15–18]. We previously developed an approach to model cell–cell interactions during human brain development by generating region-specific brain organoids, also known as spheroids, and combining them in vitro to generate 3D cellular structures called assembloids[19]. Using this approach, we modeled human interneuron migration into the cerebral cortex and identified phenotypes associated with genetic neurodevelopmental disease[19]. Although hPS cells have been differentiated into striatal neurons in two-dimensional (2D) cultures[20–22], to our knowledge, they have not been used to generate striatal 3D organoids or cortico-striatal assembloids.

Here, we first developed a protocol to generate human 3D brain organoids resembling the lateral ganglionic eminence (LGE), which gives rise to the striatum during development[23,24]. We leveraged transcriptomic trajectories of the developing human striatum and identified a small molecule that modulates the retinoic acid receptor pathway and that, in combination with WNT and activin signaling, generates 3D human striatal spheroids (hStrSs). As illustrated by single-cell RNA-sequencing (scRNA-seq) analyses and morphological analysis of cells, this approach yielded a diverse group of striatal cells, including medium spiny neurons that developed dendritic spines without a need for in vivo transplantation. Next, we assembled hStrSs with organoids resembling the cerebral cortex to form cortico-striatal assembloids (Fig. 1b). Using morphological analyses, retrograde viral tracing, live calcium imaging and patch-clamp experiments, we showed that cortical neurons in assembloids send axonal projections into hStrS and functionally connect to medium spiny neurons. Lastly, we identified functional defects in striatal neurons in assembloids derived from a cohort of patients with the 22q13.3 deletion syndrome (22q13.3DS)[25].

## Results

**Generation of 3D hStrSs.** To identify differentiation conditions that favor an LGE fate, we used two-step homology-directed repair-based genome editing to derive a reporter hiPS cell line that expresses a fluorescent protein under the promoter of the LGE-related transcription factor GSX2 (ref. [26]) (*GSX2*-mCherry; Extended Data Fig. 1). Similar to an approach we previously used to derive 3D spheroids resembling the medial ganglionic eminence (MGE)[19], we applied several small molecules at early stages of 3D neural differentiation and used the *GSX2* reporter cell line in combination with immunostaining for the early striatal marker CTIP2

[1]Department of Psychiatry and Behavioral Sciences, Stanford University, Stanford, CA, USA. [2]Human Brain Organogenesis Program, Stanford University, Stanford, CA, USA. [3]Department of Pediatrics, Stanford University, Stanford, CA, USA. ✉e-mail: spasca@stanford.edu

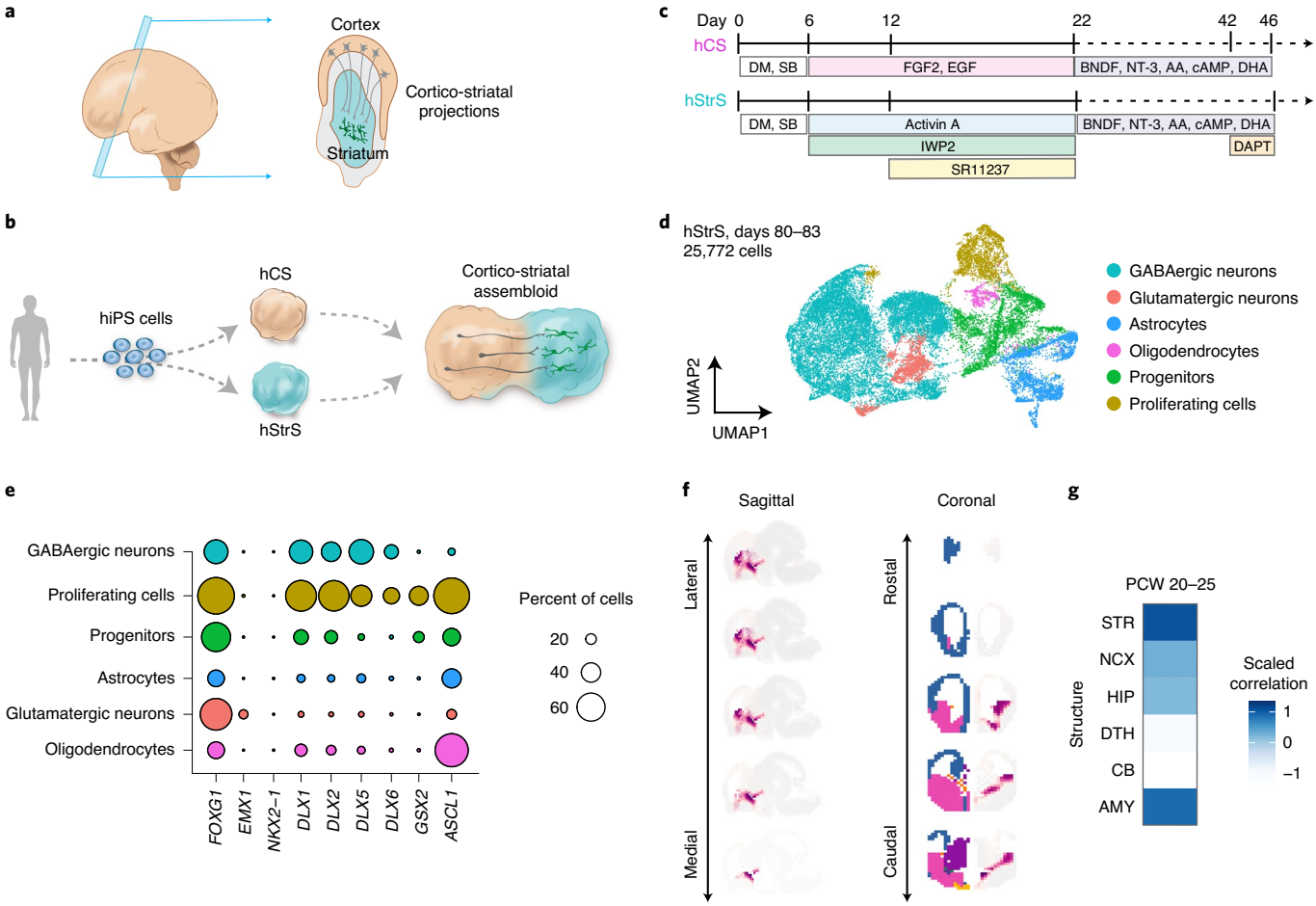


**Fig. 1 | Generation of 3D hStrSs. a**, Schematic diagram describing cortico-striatal projections in the developing human forebrain at mid-gestation. **b**, In vitro modeling of cortico-striatal projections using assembloids derived from hiPS cells. **c**, Differentiation conditions for hCSs and hStrSs. DM, dorsomorphin; SB, SB-431542; FGF2, fibroblast growth factor 2; EGF, epidermal growth factor. **d**, UMAP visualization of single-cell RNA expression in hStrSs at days 80–83 of in vitro differentiation ($n = 25{,}772$ cells from three hiPS cell lines). **e**, Dot plot shows percentage of selected markers for each cell cluster. **f**, VoxHunt spatial brain mapping of the GABAergic neuron cluster in hStrSs onto data from E13.5 mouse brains from the Allen Brain Institute. **g**, Correlation with the BrainSpan dataset of the developing human brain (PCW 20–25). STR, striatum; NCX, neocortex; HIP, hippocampus; DTH, dorsal thalamus; CB, cerebellum; AMY, amygdala.

to verify the presence of LGE cells. We generated uniform 3D spheroids by aggregating ~10,000 dissociated hiPS cells in AggreWell 800 plates. To induce neural differentiation, we applied modulators of the SMAD and WNT pathways, as well as activin A, which has been shown to promote striatal differentiation[22] (Extended Data Fig. 2a). To identify other pathways that we could modulate for LGE patterning, we inspected the BrainSpan transcriptome dataset of the developing human striatum[27]. The gene encoding retinoid X receptor gamma (*RXRG*) is one of most highly differentially expressed genes in the early developing human striatum (Extended Data Fig. 2e), and adding SR11237, a selective agonist of retinoid X receptors, in combination with the inhibitor IWP-2 and activin A (AcISr), significantly increased the proportion of $GSX2^+$ and $CTIP2^+$ cells at day 15 of differentiation as compared to human cortical spheroids (hCSs) or to cells to which only activin A was applied ($^*P = 0.01$ for hCS versus AcISr and $^*P = 0.01$ for activin versus AcISr in Extended Data Fig. 2c, $^{**}P = 0.009$ for Extended Data Fig. 2d; Extended Data Fig. 2b–d). We tested the effect of multiple concentrations of SR11237 (25 nM, 50 nM and 100 nM) on the expression of selected LGE markers by quantitative RT–PCR (RT–qPCR) (Extended Data Fig. 2f,g). We found a dose-dependent increase in *DLX5*, *BCL11B* (*CTIP2*) and *MEIS2*. We also tested an earlier exposure to SR11237 (from day 6), but this did not result in higher expression levels of LGE markers. Therefore, we proceeded by using 100 nM of SR11237 from day 12. At day 22 of in vitro differentiation, neural spheroids derived in the presence of SR11237 also showed high levels of expression of the forebrain marker *FOXG1* and LGE markers *DLX5*, *GSX2*, *BCL11B* (*CTIP2*) and *MEIS2* as compared to those from hCSs, but did not express the hypothalamic marker *RAX* or the spinal cord marker *HOXB4* ($n = 4$–9 spheroids from two to four hiPS cell lines; Extended Data Fig. 2h). Cultures were subsequently maintained in medium containing brain-derived neurotrophic factor (BDNF), neurotrophin 3 (NT-3), L-ascorbic acid 2-phosphate trisodium salt (AA), cAMP, *cis*-4,7,10,13,16,19-docosahexaenoic acid (DHA) and the Notch pathway inhibitor DAPT (Fig. 1c). We refer to neural spheroids derived by exposure to activin A, IWP-2 and SR11237 as hStrSs. A comparison with previous approaches for deriving striatal neurons in 2D is included in Supplementary Table 5.

To comprehensively study cell diversity in hStrSs, we performed droplet-based scRNA-seq analysis at days 80–83 of in vitro differentiation ($n = 25{,}772$ cells from three hiPS cell lines). Uniform Manifold Approximation and Projection (UMAP) dimensionality reduction identified six major cell clusters (Fig. 1d), including a

major group of GABAergic neurons (*STMN2*$^+$, *SYT1*$^+$) expressing the GABA-synthesizing enzyme genes *GAD1* and *GAD2* (56.99%), a cluster of dividing progenitors expressing *TOP2A* (8.67%) and one cluster of ventral forebrain progenitors expressing *GSX2*, *ASCL1* and *HOPX* (13.82%), as well astrocytes expressing *AQP4* and *GFAP* (11.58%). We also observed a small group of glutamatergic neurons expressing the glutamate transporters encoded by *SLC17A7* and *SLC17A6* (6.79%) and a cluster of oligodendrocytes expressing *SOX10* and *OLIG2* (2.12%) (Fig. 1d,e, Extended Data Fig. 3a–e and Supplementary Tables 6 and 7). Overall, the forebrain marker *FOXG1* and the ventral forebrain markers *DLX1*, *DLX2*, *DLX5* and *DLX6* were broadly expressed, while the MGE marker *NKX2-1* was only present in 0.002% of cells (Fig. 1e and Extended Data Fig. 3c), which suggests that hStrSs mostly include LGE-related cells. Cell proportions were similar across the three analyzed hiPS cell lines (with GABAergic neurons ranging from 50.12% to 66.25%), and gene expression correlations between pairs of lines were high (2242-1 versus 1205-4, $r=0.97$, $^{***}P<0.001$; 1205-4 versus 8858-3, $r=0.98$, $^{***}P<0.001$; 2242-1 versus 8858-3, $r=0.98$, $^{***}P<0.001$) (Extended Data Fig. 3f–h). To verify the regional identity of cells in hStrSs in a less biased fashion, we also mapped the scRNA-seq data onto 3D in situ hybridization data from the Allen Brain Atlas using the VoxHunt algorithm[28]. We found that the GABAergic neuron cluster in hStrSs mapped onto the ventral forebrain of the embryonic day (E) 13.5 mouse brain (Fig. 1f). In addition, we mapped data from hStrSs onto the BrainSpan human transcriptomic dataset[27]. We found that the GABAergic neuronal cluster in hStrSs showed the highest scaled correlation with ganglionic eminences (GE) when compared to primary brain samples at early stages (postconceptional weeks (PCW) 5–10) and with the striatum when compared to samples at PCW 10–25 (Fig. 1g and Extended Data Fig. 4a). We also found a correlation with the developing amygdala, which is consistent with previous reports of an LGE origin for some neurons in the amygdala[29]. In contrast, the glutamatergic neuron cluster in hStrSs was highly correlated with the neocortex and the amygdala in BrainSpan, and these cells appeared to be either dorsal forebrain- (*EMX1*$^+$) or amygdala-related (expressing the early developing amygdala marker *TFAP2D*) (Extended Data Figs. 3a,c and 4b,c). We next further analyzed the GABAergic cluster in hStrSs and found neurons expressing *SST*, *CALB1*, *CALB2*, *TH*, *NOS1* and *NPY* and only very few *PVALB*- and *CHAT*-expressing cells (Extended Data Fig. 4d,e). Immunostaining in hStrSs confirmed the expression of calbindin (CALB)1 and CALB2 (Extended Data Fig. 4f). We also compared hStrSs to our previously derived human subpallium spheroids (hSSs)[19] (Extended Data Fig. 5a–e). UMAP visualization showed that hSSs and hStrSs shared several clusters, including cluster 2 (enriched for cell proliferation markers, including *TOP2A*), cluster 4 (enriched for progenitors, including *HOPX*$^+$ cells) and clusters 6, 8 and 16 (enriched for glial lineage-related markers and expressing *S100B* and *MBP*). Clusters 10 and 13 were mostly hSS specific and expressed *LHX6* and *SST*, which are suggestive of an MGE fate[30,31]. These results suggest that hSSs (MGE-like) and hStrSs (LGE-like) display some cluster similarities, but overall, they resemble different domains of the ventral forebrain. Lastly, immunostaining of hStrSs at days 80–85 confirmed the presence of microtubule associated protein 2 (MAP2)$^+$ neurons, glial fibrillary acidic protein (GFAP)$^+$ astrocytes, myelin basic protein (MBP)$^+$ oligodendrocytes (Extended Data Fig. 5f) and achaete-scute family bHLH transcription factor 1 (ASCL1)$^+$ progenitors (Extended Data Fig. 6b) and showed cells coexpressing forkhead box P2 (FOXP2) and glutamate decarboxylase (GAD)2 (GAD65) (Extended Data Fig. 6c), GAD67 and COUP-TF-interacting protein 2 (CTIP2) and dopamine- and cAMP-regulated phosphoprotein 32 (DARPP32) and CTIP2 (Fig. 2a and Extended Data Fig. 6d), which are indicative of striatal medium spiny neurons. Overall, we found that ~50% of cells expressed CTIP2 and 8.5% expressed DARPP32 in plated hStrS cultures at day 65 (Extended Data Fig. 6e–i). Up to 30% of neuronal nuclei (NeuN)$^+$ cells expressed DARPP32 at days 80–90 in hStrSs (Fig. 2b,c; the patterns of expression of CTIP2 and DARPP32 in the E18.5 mouse striatum are shown in Extended Data Fig. 6a). We also found expression of both *DRD1* and *DRD2* in hStrSs, as well as expression of the striosome marker *TAC1* and the matrix marker *PENK* (Extended Data Fig. 6j). In addition, immunocytochemistry confirmed the expression of the D2 receptors in hStrSs at day 124 (Extended Data Fig. 6k).

Medium spiny neurons in the striatum form abundant dendritic spines during development[32]. To inspect the morphology of hStrS neurons, we labeled GABAergic cells with an adeno-associated virus (AAV) driving enhanced (e)GFP expression from a *DLX5* and *DLX6* enhancer (AAV-mDlx::eGFP[33]). In 2D-plated hStrSs, we found dendritic spines with thick spine heads as early as day 65 of differentiation (Fig. 2d and Extended Data Fig. 6e,i). In intact 3D hStrSs, the number of spines increased significantly from days 80–90 to days 120–130 ($^{****}P<0.0001$; Fig. 2e–g and Extended Data Fig. 6l,m). The number of dendritic spines did not appear to be related to differences in the proportion of glutamatergic neurons in hStrSs derived from two hiPS cell lines (Extended Data Fig. 6n).

We next examined neural activity in hStrSs, using live imaging of the genetically encoded calcium indicator GCaMP6[34]. To restrict expression to GABAergic medium spiny neurons in hStrSs, we used an AAV expressing improved Cre (iCre) under a MiniPromoter for the striatal gene *GPR88* (AAV-Ple94-iCre[35]) (Extended Data Fig. 6o). The majority of hStrS cells labeled by AAV-Ple94-iCre and AAV-EF1a::DIO-eYFP were GABAergic cells (85% GAD65$^+$, 23% GAD67$^+$) (Extended Data Fig. 6p–s). Co-infection with AAV-Ple94-iCre and AAV-EF1a::DIO-GCaMP6s, followed by live imaging of intact hStrSs, showed spontaneous calcium events that were often synchronized in an imaging field ($n=39$ cells; Fig. 2h and Supplementary Video 1). The spontaneous and synchronized calcium signals were blocked by application of the glutamate receptor antagonists NBQX and APV but not the $GABA_A$ receptor antagonist bicuculline (Extended Data Fig. 7a–e). This suggests that spontaneous activity may be related to intrinsic glutamatergic transmission in hStrSs. We also verified the gene expression of *SLC12A2* (also known as *NKCC1*) and *SLC12A5* (also known as *KCC2*), which encode cation–chloride cotransporters that regulate the developmental transition in GABAergic transmission[36]. scRNA-seq analysis at days 80–83 showed that the majority of GABAergic neurons express *KCC2*, although *NKCC1* was also expressed in some cells (Extended Data Fig. 7f). RT–qPCR experiments also showed that *NKCC1* expression decreased slightly from day 15 to day 170 (Extended Data Fig. 7g). In contrast, levels of *KCC2* expression were relatively low at early stages and increased by day 93 (Extended Data Fig. 7h).

To further examine whether hStrS neurons display characteristic electrophysiological features of striatal medium spiny neurons, we analyzed the intrinsic membrane properties of hStrS neurons. We found that 70% of hStrS cells at days 110–120 (12 of 17) showed inward rectification (Fig. 2i,j). At later stages of differentiation (days 160–170), but not at early stages (days 110–120), we found that 15% of hStrS neurons (2 of 13 cells) displayed slow-ramp depolarization with delayed first spike (Fig. 2k) and hyperpolarization of the resting membrane potential (RMP) ($-78.2\pm2.4$ mV; Fig. 2l). These properties are reminiscent of observations in postnatal medium spiny neurons in rodents[37].

**Generation of cortico-striatal assembloids.** To assemble hStrSs and hCSs, we first labeled hCSs with AAV-hSyn1::eYFP and, separately, labeled hStrSs with AAV-hSyn1::mCherry. We then placed hCSs and hStrSs in contact with each other in conical tubes, as we previously described for generating forebrain assembloids. After 72 h, the two region-specific spheroids were fused to form a

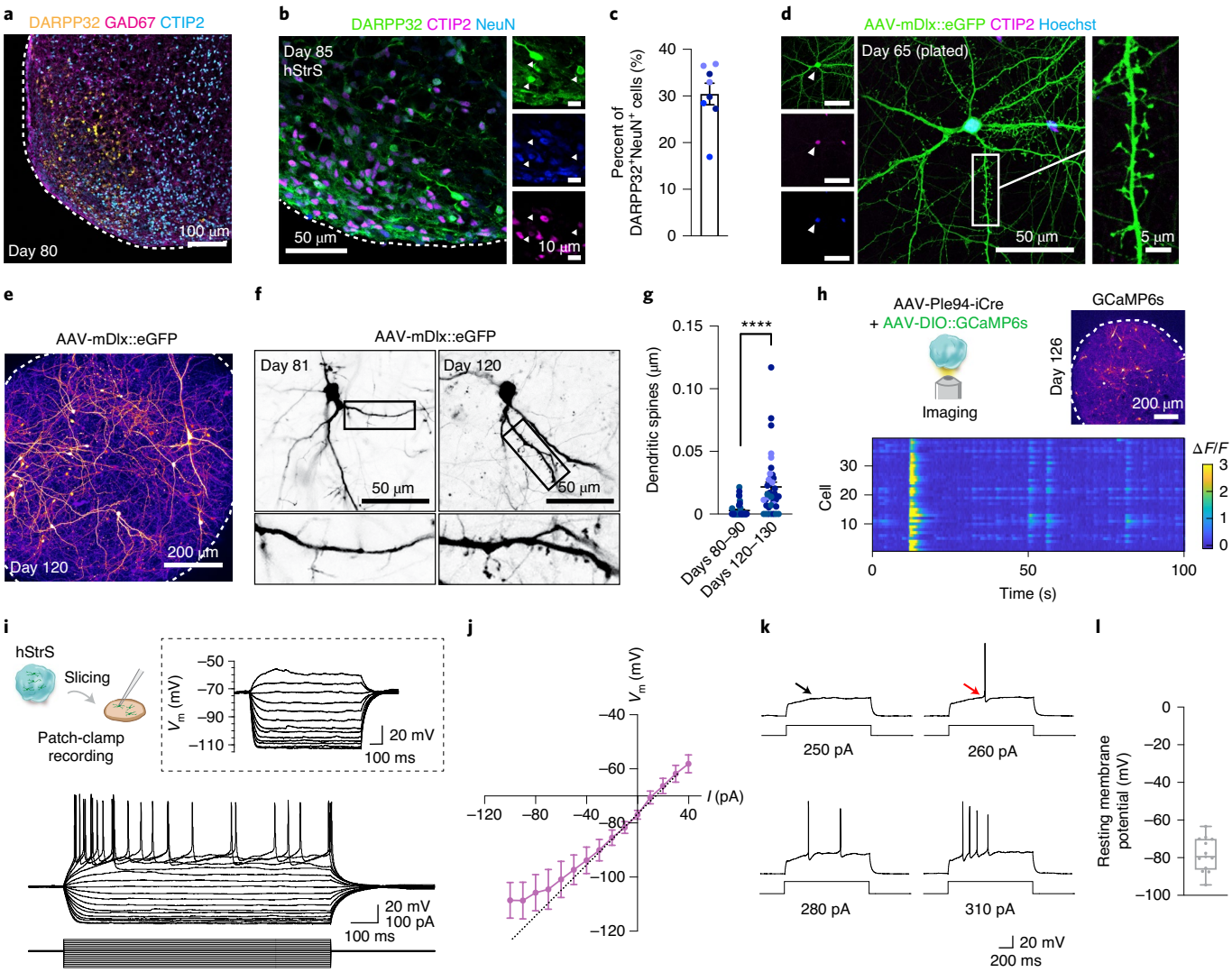


**Fig. 2 | Characterization of hStrSs. a**, Immunostaining for DARPP32 (yellow), GAD67 (magenta) and CTIP2 (cyan) in hStrSs at day 80. $n=5$ hiPS cell lines. Scale bar, 100 µm. **b**,**c**, Immunostaining for DARPP32 (green), CTIP2 (magenta) and NeuN (blue) and quantification of DARPP32$^+$ cells in hStrSs at day 85. $n=8$ neural differentiation experiments of three hiPS cell lines. **d**, Representative image showing dissociated hStrS cells labeled with the AAV-mDlx::eGFP reporter and eGFP (green), CTIP2 (magenta) and Hoechst (blue). Scale bar, 50 µm (left) and 5 µm (right). Immunostainings were repeated in dissociated hStrS cultures from four independent differentiation experiments with similar results. **e**–**g**, Dendritic spine morphology in the hStrS neurons labeled with AAV-mDlx::eGFP and quantification of the number of dendritic spines (days 80–90, $n=40$ neurons from three neural differentiation experiments of two hiPS cell lines; days 120–130, $n=38$ neurons from four differentiation experiments of three iPS cell lines; two-tailed Mann–Whitney test, $^{****}P<0.0001$). **h**, Calcium imaging of hStrS neurons expressing the genetically encoded calcium indicator GCaMP6s at day 126 of differentiation. GCaMP6s is induced by iCre expression under a MiniPromoter including the regulatory region of striatal gene *GPR88* (*Ple94*). Heatmap showing $\Delta F/F$ of GCaMP6s signal from 39 cells. Imaging was repeated in hStrSs from three independent differentiation experiments with similar results. Scale bar, 200 µm. **i**, Whole-cell patch-clamp recording and representative membrane response of hSyn1::eYFP-labeled hStrS neurons following intracellular current pulse injection. **j**, Current–frequency (*I*–*V*) curve showing inward rectification in hSyn1::eYFP$^+$ hStrS neurons ($n=17$ cells from hStrSs at days 110–120). **k**, Representative traces showing slow-ramp depolarization of hSyn1::eYFP$^+$ hStrS neurons at day 160. The black arrow indicates slow-ramp depolarization; the red arrow indicates delayed first spike. **l**, RMP ($n=13$ cells from hStrSs at days 160–170). Data show mean ± s.e.m. Box plots show maximum, third quartile, median, first quartile and minimum values.

cortico-striatal assembloid, which was subsequently transferred to an ultra-low attachment plate. Over the next 21 d, we observed a progressive increase in YFP$^+$ projections from hCSs into hStrSs ($^{**}P=0.001$ for Fig. 3c and $P=0.17$ for Fig. 3d; Fig. 3a–d, Extended Data Fig. 8a and Supplementary Video 2). Projections in hCS–hStrS were unilateral from hCSs to hStrSs (Fig. 3c) but not vice versa (Fig. 3d), a feature consistent with cortico-striatal circuits in vivo[2]. Live imaging of intact, fluorescently labeled cortico-striatal assembloids also revealed dynamic movement of growth cones from hCS neurons in hStrSs (Fig. 3e and Supplementary Video 3). Moreover, hCS eYFP$^+$ terminals within hStrSs showed expression of the glutamate transporter VGLUT1 at 21 d after fusion (daf) (Fig. 3f). Furthermore, we found projecting hCS neurons coming in close proximity to postsynaptic density protein 95 (PSD95)$^+$ puncta on dendrites of hStrS neurons (Extended Data Fig. 8b).

To identify which cortical cell types project from hCSs into hStrSs, we implemented retrograde and trans-neuronal labeling with rabies-ΔG-Cre-eGFP[38] in assembloids (Fig. 3g). Specifically, we infected hStrSs with rabies-ΔG-Cre-eGFP and AAV-EF1a::rabies glycoprotein (G), which is required for trans-synaptic spreading

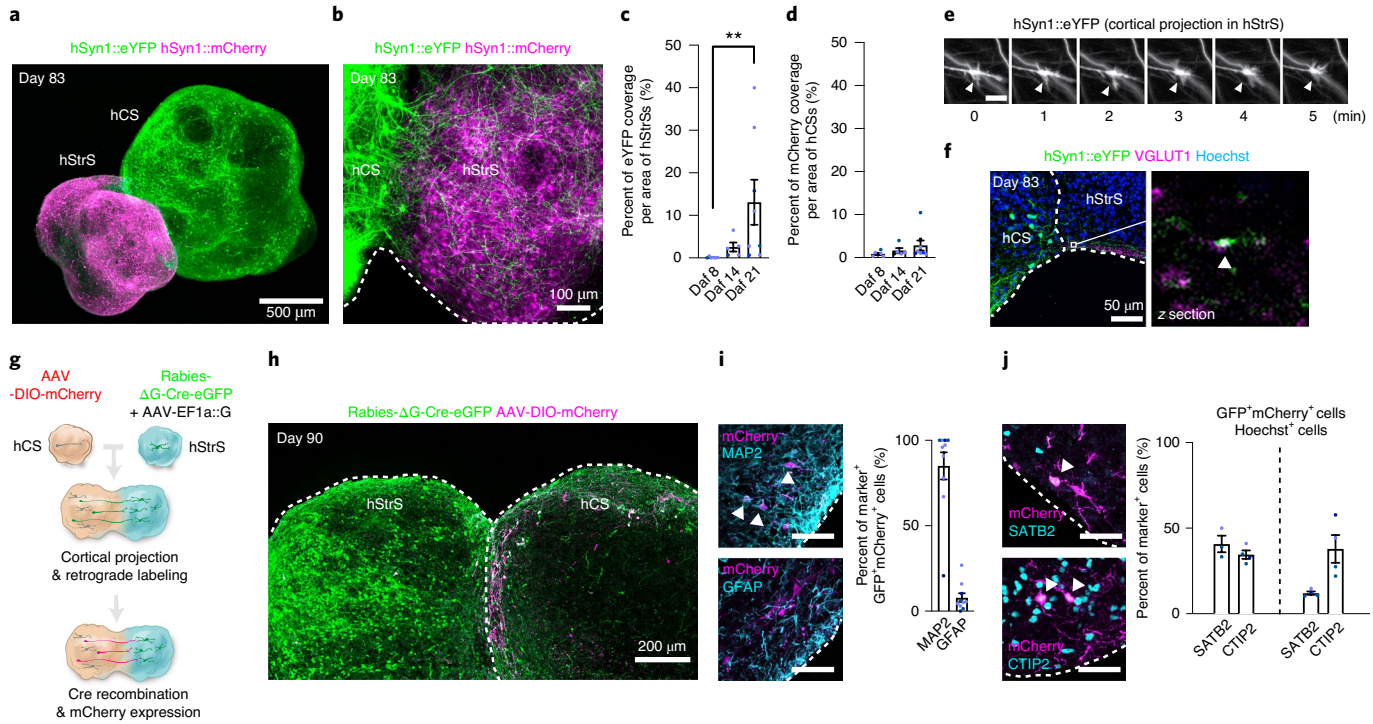


**Fig. 3 | Generation of cortico-striatal assembloids. a**, 3D immunostaining of clear, unobstructed brain–body imaging cocktails and computational analysis (CUBIC)-cleared cortico-striatal assembloids expressing AAV-hSyn1::eYFP in hCSs and AAV-hSyn1::mCherry in hStrSs (day 83). Scale bar, 500 µm. **b**, Axon projections (YFP$^+$) from hCSs into hStrSs in cortico-striatal assembloids at 21 daf (day 83 of differentiation). Scale bar, 100 µm. Quantification of percentage of eYFP fluorescence coverage per area of hStrSs (**c**) and that of mCherry fluorescence over area of hCSs (**d**). $n=6$ assembloids for daf 8, $n=5$ assembloids for daf 14 and $n=8$ assembloids for daf 21; Kruskal–Wallis test, $^{***}P=0.0002$, $^{**}P=0.001$ with Dunnett's multiple-comparison test for daf 21 versus daf 8 in **c** and Kruskal–Wallis test, $P=0.17$ for **d**. **e**, Time-lapse imaging in the hStrS side of cortico-striatal assembloids showing growth cones of hCS neurons labeled with eYFP. Arrowheads indicate the growth cone. Scale bar, 10 µm. Imaging was repeated in assembloids from three independent differentiation experiments with similar results. **f**, Representative image showing glutamatergic terminals labeled with VGLUT1 in the hStrS side of cortico-striatal assembloids. Immunostainings were repeated in assembloids from two independent differentiation experiments with similar results. **g**,**h**, Experimental design schematic and image showing retrograde viral labeling of projection neurons from hCSs into hStrSs using the rabies-ΔG-Cre-eGFP virus. Cells labeled with AAV-DIO-mCherry in hCSs that project to hStrSs and receive rabies-ΔG-Cre-eGFP retrogradely coexpress GFP and mCherry. Immunostainings were repeated in assembloids from four independent differentiation experiments with similar results. **i**, Representative image and quantitative results showing percentages of neurons (MAP2$^+$) and glial cells (GFAP$^+$) that were retrogradely labeled (GFP$^+$mCherry$^+$); $n=10$ assembloids from four differentiation experiments of three hiPS cell lines. Scale bar, 50 µm. **j**, Percentage of SATB2$^+$ or CTIP2$^+$ cells that were retrogradely labeled in the hCS side of assembloids (GFP$^+$mCherry$^+$) (left), as compared to percentages of SATB2$^+$ and CTIP2$^+$ cells out of all cells in the same slice (right); $n=3$ assembloids for SATB2$^+$GFP$^+$mCherry$^+$ cells, $n=4$ assembloids for CTIP2$^+$GFP$^+$mCherry$^+$ cells and $n=4$ assembloids for SATB2$^+$ and CTIP2$^+$Hoechst$^+$ cells from two differentiation experiments of two to three hiPS cell lines. Scale bar, 50 µm. Data show mean ± s.e.m.

of the rabies virus[39]. Separately, we infected hCSs with AAV-DIO-mCherry, which drives mCherry expression following Cre recombination. Two days after viral delivery, we assembled hCSs and hStrSs and cultured them as assembloids for another 28 d. We observed extensive expression of GFP in hStrSs and cells coexpressing GFP and mCherry on the cortical side of the assembloid (Fig. 3h), as well as mCherry$^+$ projections from hCSs into hStrSs (Extended Data Fig. 8c). We found that the majority of GFP$^+$mCherry$^+$ cells in hCSs coexpressed the neuronal marker MAP2 (85.0%), and only 7.92% expressed the glial lineage marker GFAP (Fig. 3i). A major population of neurons projecting into the striatum is composed of cortical intratelencephalic projection neurons expressing the transcription factor SATB2. Deep-layer CTIP2$^+$ cortical neurons of the pyramidal tract also send important collaterals into the striatum[2,40,41]. We found a 3.4× enrichment in the proportion of SATB2$^+$ cells in the GFP$^+$mCherry$^+$ population compared to all other cells in the same section of hCSs ($^*P=0.01$), and, overall, ~41% of the retrogradely labeled hCS neurons were SATB2$^+$ (Fig. 3j). CTIP2$^+$ cells accounted for ~34% of GFP$^+$mCherry$^+$ cells. We note that some cells in hCSs expressed GFP in the absence of mCherry, and this may be due to differences in viral transduction in hCSs (AAV-based) and hStrSs (rabies-based). Although there are still technical challenges with tracing connectivity[42], including ascertaining trans-synaptic tracing with rabies virus, these data suggest that projection neurons in assembloids are biased toward certain neuronal populations.

**Functional neural circuits in cortico-striatal assembloids.** To determine whether neurons projecting from hCSs can form functional synaptic connections with hStrS neurons, we implemented optogenetics with simultaneous calcium imaging in cortico-striatal assembloids. To detect optically evoked calcium responses, we first virally expressed hSyn1::ChrimsonR–tdTomato in hCSs, an opsin that excites neurons in response to red-shifted light[43], and separately in hStrSs, we delivered Ple94-iCre and DIO-GCaMP6s (Fig. 4a). After 2 d of viral infection, we assembled hCSs and hStrSs and imaged them around day 90 of differentiation (Fig. 4b). We found that the application of 625-nm light reliably elicited calcium responses in hStrS cells (Fig. 4c,d). The median $\Delta F/F$ of GCaMP6 signals was significantly higher following light

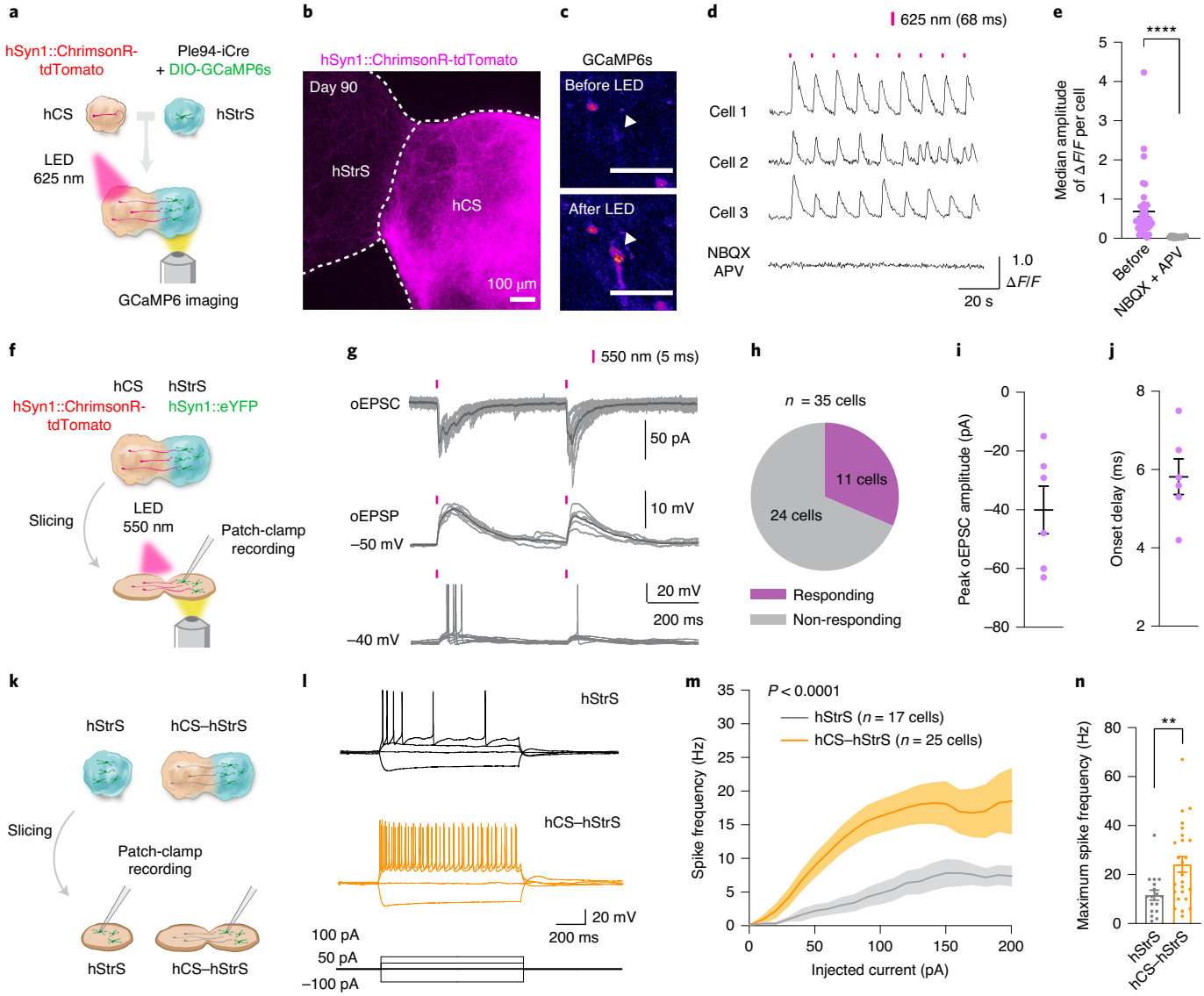


**Fig. 4 | Functional neural circuits in cortico-striatal assembloids. a**, Optogenetics coupled with calcium imaging of the cortico-striatal assembloid. hCSs expressing AAV-ChrimsonR-tdTomato and hStrSs expressing AAV-Ple94-iCre and AAV-EF1a::DIO-GCaMP6s were assembled. GCaMP6-expressing neurons in hStrSs were imaged by stimulating with 625-nm LED light (68 ms) at days 90–145 of differentiation. **b**, Axon projection of ChrimsonR-tdTomato-expressing neurons from hCSs to hStrSs of cortico-striatal assembloids at day 90. Scale bar, 100 µm. Imaging was repeated in assembloids from one differentiation experiment. **c**, Cells in hStrSs responding to stimulation with 625-nm LED light. Scale bar, 50 µm. Imaging was repeated in assembloids from five independent differentiation experiments with similar results. Representative traces of GCaMP6s imaging (**d**) and median amplitudes of $\Delta F/F$ per cell before and during NBQX (20 µM) and APV (50 µM) treatment (**e**). $n = 36$ cells for before treatment with NBQX and APV and $n = 17$ cells for during treatment with NBQX and APV; two-tailed Mann–Whitney test, $^{****}P < 0.0001$. **f**, Schematic diagram illustrating the method for whole-cell patch-clamp recording with optogenetic activation in cortico-striatal assembloids. **g**, Representative traces of oEPSCs, oEPSPs and neuronal firing of hStrS neurons stimulated by LED light (5-ms duration of 550-nm whole-field LED illumination). Percentage of responsive cells (11 of 35 cells) (**h**), peak oEPSC amplitudes (**i**) and onset delays ($n = 6$ cells) (**j**) of hStrS neurons in cortico-striatal assembloids. **k**, Schematic showing whole-cell patch-clamp recording in hStrSs or cortico-striatal assembloids in slices. **l**, Representative electrophysiological traces of neurons in hStrSs and hCS-hStrS. **m**, Frequency–current ($F$–$I$) curves showing spike frequency versus current injected in hStrSs and hCS-hStrS neurons ($n = 17$ cells in hStrSs, $n = 25$ cells in hCS-hStrS from three hiPS cell lines; two-way ANOVA, $F_{1,840} = 131.6$, $^{****}P < 0.0001$ for current injection). **n**, Maximum spike frequency ($n = 17$ cells in hStrSs, $n = 25$ cells in hCS-hStrS from three hiPS cell lines; two-tailed unpaired $t$-test, $^{**}P = 0.005$). Data show mean ± s.e.m.

stimulation as compared to the median $\Delta F/F$ at randomly selected time points ($n = 180$ cells, $^{***}P = 0.0002$, Extended Data Fig. 8d,e). Responding cells were also able to respond to different frequencies of light in sequential stimulation experiments (Extended Data Fig. 8f). We also observed, however, non-responding cells or cells that fired spontaneously during optogenetic stimulation (Fig. 4d and Extended Data Fig. 8e). Lastly, light-induced calcium responses were blocked by application of the α-amino-3-hydroxy-5-methyl-4-isoxazolepropionic acid (AMPA) receptor antagonist NBQX (20 µM) and the NMDA (*N*-methyl-D-aspartate) receptor antagonist APV (50 µM) ($^{****}P < 0.0001$; Fig. 4d,e), and this effect was reversible (Extended Data Fig. 8g), suggesting that some of these calcium signals were mediated by glutamatergic transmission from hCSs to hStrSs. In addition, light-emitting diode (LED) exposure, in

the absence of an opsin in hCSs, did not induce calcium responses in cortico-striatal assembloids (Extended Data Fig. 8h,i). We also quantified the median amplitude of $\Delta F/F$ GCaMP6 signals over time in hStrSs and found an increase in the amplitude of optically evoked GCaMP6 signals at days 100–120 and at days 140–150 as compared to hStrSs before day 100 (Extended Data Fig. 8j). This result suggests that there may be a time-dependent increase in the strength or frequency of synaptic connections in cortico-striatal assembloids.

To further characterize connectivity in cortico-striatal assembloids, we combined optogenetic stimulation with electrophysiological whole-cell recording in slices (Fig. 4f). We found that delivery of 550-nm light stimulation could induce optically evoked excitatory postsynaptic currents (oEPSCs) and optically evoked excitatory postsynaptic potentials (oEPSPs), as well as firing of neurons in hStrSs (Fig. 4g). The success rate was moderately high, with 11 of 35 recorded cells (Fig. 4h) responding with approximately 40 pA of average oEPSC amplitude (Fig. 4i) and 6 ms of onset delay (Fig. 4j). This indicates that neurons in hStrSs can synaptically connect with hCS projecting neurons in cortico-striatal assembloids.

Glutamatergic projections from the cerebral cortex into the striatum are thought to play a key role in the developmental maturation of medium spiny neurons[32]. To examine whether the assembly of hCSs and hStrSs impacts the electrophysiological properties of neurons in hStrSs, we performed whole-cell patch-clamp recordings in sliced cortico-striatal assembloids (Fig. 4k). We found increased intrinsic excitability of hSyn1::eYFP-labeled neurons on the hStrS side of hCS–hStrS, as compared to neurons in hStrSs at the same in vitro stage ($P<0.0001$, $^{**}P=0.005$; Fig. 4l–n). We also analyzed individual action potentials and found shorter spike half-widths in hCS–hStrS neurons without a change in the amplitude or spike threshold (Extended Data Fig. 9a–h), which is consistent with findings in the developing murine striatum[44]. Neither capacitance nor input resistance was changed ($P=0.68$ for Extended Data Fig. 9i, $P=0.82$ for Extended Data Fig. 9j; Extended Data Fig. 9i,j), suggesting that the physiological change was not due to differences in the cell size or surface area of patched cells. Moreover, the RMPs were also not changed before or after assembly ($P=0.87$; Extended Data Fig. 9k). We also observed a higher frequency of spontaneous EPSCs (sEPSCs) in hStrS neurons following assembly ($^{***}P=0.0006$; Extended Data Fig. 9l,m), while the number of dendritic spines in hStrS neurons was not changed following assembly (Extended Data Fig. 9n), suggesting that assembly with hCSs may not affect the morphology of hStrS neurons. In sum, these results indicate that functional connectivity can be assessed in cortico-striatal assembloids derived from hiPS cells in vitro and that this assembly results in changes of intrinsic firing properties in hStrSs.

**Modeling disease-related cellular phenotypes in cortico-striatal assembloids.** Lastly, we studied whether cortico-striatal assembloids could be used to model cellular defects associated with genetic neurodevelopmental disease. Phelan–McDermid syndrome, also known as 22q13.3DS, is a severe disorder characterized by global developmental delay, severe intellectual impairment, delayed speech and ASD. The syndrome is caused by a deletion on chromosome 22q13.3 that includes the *SHANK3* gene, which encodes a key postsynaptic scaffold protein[25]. SHANK3 is highly expressed in the striatum and considered to be essential for cortico-striatal circuit development and function, and its loss is considered to be a key player in the pathogenesis of 22q13.3DS[4,37,45–48]. Defects in cortico-striatal connectivity were previously suggested in *Shank3*-knockout mice[37]. However, whether cellular abnormalities are present in heterozygous human cells in cortico-striatal circuits from patients is not known. To investigate whether we could model cortico-striatal defects in 22q13.3DS, we first differentiated hiPS cell lines from three patients with 22q13.3DS into hCSs and, separately, into hStrSs (Fig. 5a; characterization of hiPS cells including morphology, pluripotency marker expression and genome integrity and microdeletion ascertainment by single-nucleotide polymorphism (SNP) arrays are shown in Fig. 5b and Extended Data Fig. 10a–c). We found that patient-derived hiPS cells could efficiently aggregate and differentiate in 3D cultures to form hStrSs (Fig. 5b and Extended Data Fig. 10d) and, as expected, expressed the forebrain marker *FOXG1* and the LGE markers *GSX2*, *MEIS2* and *BCL11B* (*CTIP2*), but not the spinal cord marker *HOXB4* (Extended Data Fig. 10e). The area of hCSs and hStrSs derived from patients with 22q13.3DS was not different from that of controls (Fig. 5c), and all 22q13.3DS lines could efficiently generate DARPP32$^{+}$NeuN$^{+}$ neurons (Fig. 5d and Extended Data Fig. 10f). We next generated cortico-striatal assembloids from three patients with 22q13.3DS and three control individuals and performed calcium imaging (Fig. 5e–g). We found that 22q13.3DS-derived neurons labeled with AAV-mDlx::GCaMP6f in the hStrS side of cortico-striatal assembloids displayed increased number of calcium spike events ($^{*}P=0.01$; Fig. 5e–g). Notably, when tested at the same stage of in vitro differentiation, this defect was not present in hStrSs derived from patients with 22q13.3DS ($P=0.54$; Fig. 5h–j). To follow up on these changes in global calcium events in 22q13.3DS-derived hStrSs and cortico-striatal assembloids, we used GCaMP6 signals to calculate mean correlation coefficients between cells. We found reduced network synchronization in both hStrSs and cortico-striatal

**Fig. 5 | Modeling altered neural activity in cortico-striatal assembloids derived from patients with 22q13.3DS. a**, Schematic illustrating the generation of hCSs and hStrSs derived from control and 22q13.3DS hiPS cells. **b**, Representative images of 3D neural spheroids (at day 5) derived from control and 22q13.3DS hiPS cell lines. Scale bars, 1 mm. **c**, Quantification of the area of hCSs and hStrSs derived from control and 22q13.3DS cells at days 87–145; $n=40$ spheroids for control hCSs, $n=25$ spheroids for 22q13.3DS hCSs, $n=94$ spheroids for control hStrSs, $n=51$ 22q13.3DS spheroids from four differentiation experiments of three hiPS cell lines for controls and three hiPS cell lines for 22q13.3DS cells; one-way ANOVA, $F_{3,8}=3.2$, $P=0.07$. **d**, Immunostaining for DARPP32 (green), CTIP2 (magenta) and NeuN (blue) in hStrSs derived from 22q13.3DS cells at day 85; $n=3$ hiPS cell lines. Scale bar, 50 µm. **e**, Schematic showing the functional characterization of cortico-striatal assembloids derived from patients with 22q13.3DS. **f**,**g**, Calcium imaging of hStrS neurons labeled with AAV-mDlx::GCaMP6f in hCS–hStrS (day 80, 18 daf) derived from control participants and patients with 22q13.3DS and quantitative results showing the number of $Ca^{2+}$ events per minute ($n=142$ control cells from ten assembloids with three hiPS cell lines, $n=164$ 22q13.3DS cells from eight assembloids with three hiPS cell lines; two-tailed unpaired *t*-test, $^{*}P=0.01$). **h**, Schematic illustrating the calcium imaging of hStrSs derived from patients with 22q13.3DS. **i**,**j**, Calcium imaging of hStrS neurons labeled with AAV-mDlx::GCaMP6f (day 80, 18 daf) derived from control individuals and patients with 22q13DS and quantitative results showing the number of $Ca^{2+}$ events per minute ($n=91$ control cells from four assembloids with three hiPS cell lines, $n=143$ 22q13.3DS cells from six assembloids with three hiPS cell lines; two-tailed unpaired *t*-test, $P=0.54$. **k**, Heatmap showing mean correlation coefficient of $\Delta F/F$ values of GCaMP6 per pair of cells in cortico-striatal assembloids from control (left) and 22q13.3DS (right) cells. Quantification in cortico-striatal assembloids (**l**) and spheroids (**m**). $n=127$ cells for control cells from seven assembloids and $n=173$ cells for 22q13.3DS cells from eight assembloids; two-tailed, unpaired *t*-test, $^{****}P<0.0001$ in **l**. $n=86$ cells for control cells from four spheroids and $n=168$ cells for 22q13.3DS cells from six spheroids; two-tailed, unpaired *t*-test, $^{*}P=0.01$ in **m**. Data shown are mean ± s.e.m. Gray dots indicate cells, small colored dots show spheroids or assembloids, and large colored dots show different hiPS cell lines in **c**,**g**,**j**,**l**,**m**.

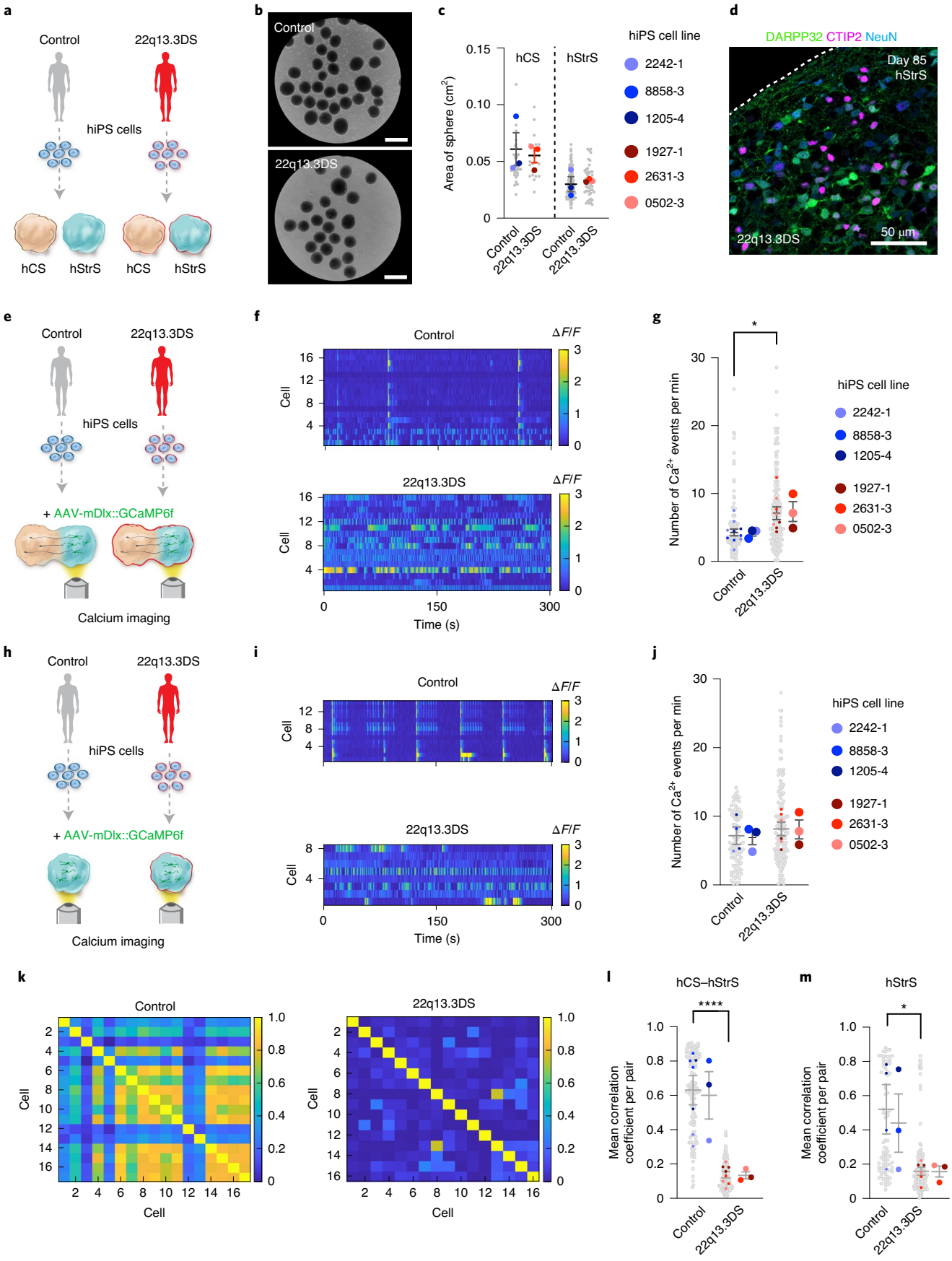
a
Control
22q13.3DS
hiPS cells
hCS
hStrS
hCS
hStrS
b
Control
22q13.3DS
c
hCS
hStrS
Area of sphere (cm²)
0.15
0.10
0.05
0
Control
22q13.3DS
Control
22q13.3DS
hiPS cell line
2242-1
8858-3
1205-4
1927-1
2631-3
0502-3
d
DARPP32 CTIP2 NeuN
Day 85
hStrS
22q13.3DS
50 µm
e
Control
22q13.3DS
hiPS cells
+ AAV-mDlx::GCaMP6f
Calcium imaging
f
Control
ΔF/F
Cell
22q13.3DS
Time (s)
g
Number of Ca²⁺ events per min
Control
22q13.3DS
hiPS cell line
2242-1
8858-3
1205-4
1927-1
2631-3
0502-3
h
Control
22q13.3DS
hiPS cells
+ AAV-mDlx::GCaMP6f
Calcium imaging
i
Control
ΔF/F
Cell
22q13.3DS
Time (s)
j
Number of Ca²⁺ events per min
Control
22q13.3DS
hiPS cell line
2242-1
8858-3
1205-4
1927-1
2631-3
0502-3
k
Control
22q13.3DS
Cell
l
hCS–hStrS
Mean correlation coefficient per pair
Control
22q13.3DS
m
hStrS
Mean correlation coefficient per pair
Control
22q13.3DS

assembloids derived from patients with 22q13.3DS (****$P < 0.0001$ in Fig. 5l, *$P < 0.01$ in Fig. 5m; Fig. 5k–m). In sum, these results indicate that cortico-striatal assembloids can be used to recapitulate the altered neural activity of human cells in disease.

## Discussion

In this study, we generated human 3D striatal cultures that include morphologically and functionally mature striatal neurons that can be assembled with cortical glutamatergic projection neurons to model human cortico-striatal circuits in vitro. Classical ex vivo explant experiments[49] and, more recently, in vivo functional studies in behaving animals[50] serve as critical experimental models to functionally interrogate cortico-striatal pathways and to model disease in knockout animals. To date, however, there are no cellular models that allow these cell–cell interactions to be validated in a functional human preparation while also taking into account the complex genetic architecture of basal ganglia disorders. Previous methods of deriving striatal neurons from hPS cells have yielded relatively immature cells, which has limited their application to disease modeling[21,22]. Although the proportion of neurons in hStrSs is not as high as that in conventional striatal 2D cultures[21,22], we found that neurons in hStrSs form abundant dendritic spines and recapitulate intrinsic electrophysiological properties described in rodent medium spiny neurons. Moreover, assembly of hStrSs with cortical neurons accelerates the intrinsic functional maturation of striatal neurons, which could be due to glutamate release following assembly, mediated through NMDA receptor activation and subsequent modulation of potassium channel function[51]. Future studies could investigate whether assembly with midbrain organoids producing dopamine in three-part assembloids could even further advance their electrophysiological properties[52].

The main advantage of our approach is its modularity. Cortical neurons, but not neurons in striatal 3D cultures, project into the counterpart spheroid, which is reminiscent of the directionality of this pathway in vivo[2]. To probe the functionality of this 3D human cellular model, we implemented rabies virus tracing and optogenetic stimulation coupled with live imaging of genetically encoded calcium indicators delivered to specific cell types. Notably, we found that projecting cortical neurons were biased to express a marker for intratelencephalic projecting neurons, although a considerable fraction of these expressed a marker of corticofugal neurons, which send collaterals toward the basal ganglia[2]. Moreover, optogenetic stimulation of cortical neurons can reliably trigger calcium activity or even action potentials in medium spiny neurons in cortico-striatal assembloids, which are mediated by glutamate transmission. Although more studies using orthogonal mapping methods are required, these experiments suggest that connectivity with some level of specificity is possible in vitro. Future experiments should also explore whether selective cortical connectivity through dopamine receptor D1 or D2 pathways can be intrinsically achieved in vitro or if activity through the cortico-striatal-thalamic loop is required for this selectivity.

Modeling cytoarchitectural features of specific brain regions in vitro is a central goal of brain organoid research. Although we did not directly observe striosomes or other matrix structures that are present in the striatum[53], it remains to be seen whether these features can organize at later stages of maturation in vitro, following midbrain assembly or, perhaps, as a consequence of broader circuit input after in vivo transplantation in rodents. Alternatively, it could be that embedding organizer-like structures, such as organoids secreting sonic hedgehog[54], may induce spatial organization in hStrSs.

Our system has a number of potential applications for the study of human striatal development and the pathophysiology of diseases of cortico-striatal circuits. Here we used this system to capture cellular defects associated with 22q13.3DS, in which the postsynaptic, striatum-enriched *SHANK3* gene is hemizygously deleted. Previous work in homozygous knockout rodent models suggested potential functional defects in the cortico-striatal pathway. Indeed, we found that while hStrSs displayed similar spontaneous calcium activity in the 22q13.3DS background as compared to controls, following assembly with hCSs, medium spiny neurons become hyperactive in patient-derived cultures. This increase in intrinsic neuronal activity is in line with previously reported defects in mouse and human cortical neurons[37,55], although a functional cellular defect in human striatal cells in the 22q13.3DS background has not been reported. Future studies should use more patients to test these defects in the context of various 22q13.3 chromosomal deletions and identify the role of *SHANK3*, establish whether this phenotype is cell-intrinsic (using hybrid assembloids as we previously showed for forebrain assembloids[19]) and discover the specific contribution of cortical glutamatergic neurons to dysfunction in assembloids derived from patients with disease. We found network synchronization changes in 22q13.3DS cells in assembloids as well as in hStrSs. Future studies should investigate how this phenotype is related to cell composition in hStrSs. Notably, *Shank3*$^{-/-}$ mice display a reduction in the density of dendritic spines in the striatum as well as changes in glutamate receptor expression, which are related to an increase in dendritic length[4]. Therefore, it is possible that changes in cell morphology and synaptic function in patient-derived medium spiny neurons could also contribute to network alterations in 22q13.3DS cells.

In addition to uncovering the molecular mechanism underlying the assembly-dependent cellular defect following the loss of SHANK3, our system should be useful for modeling other neuropsychiatric disorders of the cortico-striatal circuit, including Tourette syndrome, ASD and obsessive–compulsive disorder[3]. Moreover, it may allow the investigation of trans-neuronal cortico-striatal spreading of huntingtin in Huntington's disease[56]. Ultimately, circuits built in assembloids generated by combining various region-specific brain organoids may advance our understanding of neuronal connectivity in disease and accelerate the search for novel therapeutics for neuropsychiatric disorders.

## Online content

Any methods, additional references, Nature Research reporting summaries, source data, extended data, supplementary information, acknowledgements, peer review information; details of author contributions and competing interests; and statements of data and code availability are available at https://doi.org/10.1038/s41587-020-00763-w.

Received: 11 May 2020; Accepted: 2 November 2020;
Published online: 3 December 2020

## References

1. Alexander, G. E., DeLong, M. R. & Strick, P. L. Parallel organization of functionally segregated circuits linking basal ganglia and cortex. *Annu. Rev. Neurosci.* **9**, 357–381 (1986).
2. Shepherd, G. M. Corticostriatal connectivity and its role in disease. *Nat. Rev. Neurosci.* **14**, 278–291 (2013).
3. Milad, M. R. & Rauch, S. L. Obsessive-compulsive disorder: beyond segregated cortico-striatal pathways. *Trends Cogn. Sci.* **16**, 43–51 (2012).
4. Peca, J. et al. *Shank3* mutant mice display autistic-like behaviours and striatal dysfunction. *Nature* **472**, 437–442 (2011).
5. Welch, J. M. et al. Cortico-striatal synaptic defects and OCD-like behaviours in *Sapap3*-mutant mice. *Nature* **448**, 894–900 (2007).
6. Amin, N. D. & Pasca, S. P. Building models of brain disorders with three-dimensional organoids. *Neuron* **100**, 389–405 (2018).
7. Sasai, Y. Cytosystems dynamics in self-organization of tissue architecture. *Nature* **493**, 318–326 (2013).
8. Pasca, S. P. The rise of three-dimensional human brain cultures. *Nature* **553**, 437–445 (2018).
9. Eiraku, M. et al. Self-organized formation of polarized cortical tissues from ESCs and its active manipulation by extrinsic signals. *Cell Stem Cell* **3**, 519–532 (2008).

10. Mariani, J. et al. Modeling human cortical development in vitro using induced pluripotent stem cells. *Proc. Natl Acad. Sci. USA* **109**, 12770–12775 (2012).
11. Lancaster, M. A. et al. Cerebral organoids model human brain development and microcephaly. *Nature* **501**, 373–379 (2013).
12. Pasca, A. M. et al. Functional cortical neurons and astrocytes from human pluripotent stem cells in 3D culture. *Nat. Methods* **12**, 671–678 (2015).
13. Qian, X. et al. Brain-region-specific organoids using mini-bioreactors for modeling ZIKV exposure. *Cell* **165**, 1238–1254 (2016).
14. Marton, R. M. et al. Differentiation and maturation of oligodendrocytes in human three-dimensional neural cultures. *Nat. Neurosci.* **22**, 484–491 (2019).
15. Bershteyn, M. et al. Human iPSC-derived cerebral organoids model cellular features of lissencephaly and reveal prolonged mitosis of outer radial glia. *Cell Stem Cell* **20**, 435–449 (2017).
16. Klaus, J. et al. Altered neuronal migratory trajectories in human cerebral organoids derived from individuals with neuronal heterotopia. *Nat. Med.* **25**, 561–568 (2019).
17. Blair, J. D., Hockemeyer, D. & Bateup, H. S. Genetically engineered human cortical spheroid models of tuberous sclerosis. *Nat. Med.* **24**, 1568–1578 (2018).
18. Pasca, A. M. et al. Human 3D cellular model of hypoxic brain injury of prematurity. *Nat. Med.* **25**, 784–791 (2019).
19. Birey, F. et al. Assembly of functionally integrated human forebrain spheroids. *Nature* **545**, 54–59 (2017).
20. Ma, L. et al. Human embryonic stem cell-derived GABA neurons correct locomotion deficits in quinolinic acid-lesioned mice. *Cell Stem Cell* **10**, 455–464 (2012).
21. Delli Carri, A. et al. Developmentally coordinated extrinsic signals drive human pluripotent stem cell differentiation toward authentic DARPP-32$^{+}$ medium-sized spiny neurons. *Development* **140**, 301–312 (2013).
22. Arber, C. et al. Activin A directs striatal projection neuron differentiation of human pluripotent stem cells. *Development* **142**, 1375–1386 (2015).
23. Watson, C., Paxinos, G. & Puelles, L. *The Mouse Nervous System* 1st edn (Elsevier Academic Press, 2012).
24. Onorati, M. et al. Molecular and functional definition of the developing human striatum. *Nat. Neurosci.* **17**, 1804–1815 (2014).
25. Phelan, K. & McDermid, H. E. The 22q13.3 deletion syndrome (Phelan–McDermid syndrome). *Mol. Syndromol.* **2**, 186–201 (2012).
26. Yun, K., Potter, S. & Rubenstein, J. L. Gsh2 and Pax6 play complementary roles in dorsoventral patterning of the mammalian telencephalon. *Development* **128**, 193–205 (2001).
27. Kang, H. J. et al. Spatio-temporal transcriptome of the human brain. *Nature* **478**, 483–489 (2011).
28. Fleck, J. S., He, Z., Boyle, M. J., Camp, J. G. & Treutlein, B. Resolving brain organoid heterogeneity by mapping single cell genomic data to a spatial reference. Preprint at *bioRxiv* https://doi.org/10.1101/2020.01.06.896282 (2020).
29. Waclaw, R. R., Ehrman, L. A., Pierani, A. & Campbell, K. Developmental origin of the neuronal subtypes that comprise the amygdalar fear circuit in the mouse. *J. Neurosci.* **30**, 6944–6953 (2010).
30. Hu, J. S., Vogt, D., Sandberg, M. & Rubenstein, J. L. Cortical interneuron development: a tale of time and space. *Development* **144**, 3867–3878 (2017).
31. Silberberg, S. N. et al. Subpallial enhancer transgenic lines: a data and tool resource to study transcriptional regulation of GABAergic cell fate. *Neuron* **92**, 59–74 (2016).
32. Steiner, H. & Tseng, K.-Y. *Handbook of Basal Ganglia Structure and Function* 2nd edn (Elsevier Academic Press, 2017).
33. Dimidschstein, J. et al. A viral strategy for targeting and manipulating interneurons across vertebrate species. *Nat. Neurosci.* **19**, 1743–1749 (2016).
34. Chen, T. W. et al. Ultrasensitive fluorescent proteins for imaging neuronal activity. *Nature* **499**, 295–300 (2013).
35. de Leeuw, C. N. et al. rAAV-compatible MiniPromoters for restricted expression in the brain and eye. *Mol. Brain* **9**, 52 (2016).
36. Blaesse, P., Airaksinen, M. S., Rivera, C. & Kaila, K. Cation-chloride cotransporters and neuronal function. *Neuron* **61**, 820–838 (2009).
37. Peixoto, R. T., Wang, W., Croney, D. M., Kozorovitskiy, Y. & Sabatini, B. L. Early hyperactivity and precocious maturation of corticostriatal circuits in *Shank3B*$^{-/-}$ mice. *Nat. Neurosci.* **19**, 716–724 (2016).
38. Wickersham, I. R., Finke, S., Conzelmann, K. K. & Callaway, E. M. Retrograde neuronal tracing with a deletion-mutant rabies virus. *Nat. Methods* **4**, 47–49 (2007).
39. Etessami, R. et al. Spread and pathogenic characteristics of a G-deficient rabies virus recombinant: an in vitro and in vivo study. *J. Gen. Virol.* **81**, 2147–2153 (2000).
40. Wilson, C. J. Morphology and synaptic connections of crossed corticostriatal neurons in the rat. *J. Comp. Neurol.* **263**, 567–580 (1987).
41. Sohur, U. S., Padmanabhan, H. K., Kotchetkov, I. S., Menezes, J. R. & Macklis, J. D. Anatomic and molecular development of corticostriatal projection neurons in mice. *Cereb. Cortex* **24**, 293–303 (2014).
42. Luo, L., Callaway, E. M. & Svoboda, K. Genetic dissection of neural circuits: a decade of progress. *Neuron* **98**, 256–281 (2018).
43. Klapoetke, N. C. et al. Independent optical excitation of distinct neural populations. *Nat. Methods* **11**, 338–346 (2014).
44. Belleau, M. L. & Warren, R. A. Postnatal development of electrophysiological properties of nucleus accumbens neurons. *J. Neurophysiol.* **84**, 2204–2216 (2000).
45. Peixoto, R. T. et al. Abnormal striatal development underlies the early onset of behavioral deficits in *Shank3B*$^{-/-}$ mice. *Cell Rep.* **29**, 2016–2027 (2019).
46. Zhou, Y. et al. Atypical behaviour and connectivity in *SHANK3*-mutant macaques. *Nature* **570**, 326–331 (2019).
47. Misceo, D. et al. A translocation between Xq21.33 and 22q13.33 causes an intragenic *SHANK3* deletion in a woman with Phelan–McDermid syndrome and hypergonadotropic hypogonadism. *Am. J. Med. Genet.* **155**, 403–408 (2011).
48. Shcheglovitov, A. et al. SHANK3 and IGF1 restore synaptic deficits in neurons from 22q13 deletion syndrome patients. *Nature* **503**, 267–271 (2013).
49. Plenz, D. & Aertsen, A. Neural dynamics in cortex-striatum co-cultures—I. anatomy and electrophysiology of neuronal cell types. *Neuroscience* **70**, 861–891 (1996).
50. Bloem, B., Huda, R., Sur, M. & Graybiel, A. M. Two-photon imaging in mice shows striosomes and matrix have overlapping but differential reinforcement-related responses. *eLife* **6**, e32353 (2017).
51. Shi, M. et al. Effects of NR2A and NR2B-containing *N*-methyl-D-aspartate receptors on neuronal-firing properties. *Neuroreport* **22**, 762–766 (2011).
52. Lieberman, O. J. et al. Dopamine triggers the maturation of striatal spiny projection neuron excitability during a critical period. *Neuron* **99**, 540–554 (2018).
53. Graybiel, A. M. & Ragsdale, C. W. Jr. Histochemically distinct compartments in the striatum of human, monkeys, and cat demonstrated by acetylthiocholinesterase staining. *Proc. Natl Acad. Sci. USA* **75**, 5723–5726 (1978).
54. Cederquist, G. Y. et al. Specification of positional identity in forebrain organoids. *Nat. Biotechnol.* **37**, 436–444 (2019).
55. Yi, F. et al. Autism-associated SHANK3 haploinsufficiency causes Ih channelopathy in human neurons. *Science* **352**, aaf2669 (2016).
56. Pecho-Vrieseling, E. et al. Transneuronal propagation of mutant huntingtin contributes to non-cell autonomous pathology in neurons. *Nat. Neurosci.* **17**, 1064–1072 (2014).

## Methods

**Characterization and maintenance of hiPS cells.** hiPS cell lines used in this study were validated using standardized methods as previously described[57]. Cultures were frequently tested for mycoplasma and maintained free of mycoplasma. A total of five control hiPS cell lines derived from fibroblasts collected from five healthy individuals and three hiPS cell lines derived from fibroblasts collected from three patients with 22q13.3DS were used for experiments (Supplementary Table 3). Approval for this study was obtained from the Stanford IRB panel, and informed consent was obtained from all participants.

**Genome-wide SNP genotyping of hiPS cells.** Genome-wide SNP genotyping was performed using the Illumina genome-wide GSAMD-24 version 2.0 SNP microarray at the Children's Hospital of Philadelphia. B-allele frequency and probe-level log R ratio were generated using the Illumina GenomeStudio software (version 2.0.4).

**Generation of *GSX2*-mCherry hiPS cells using CRISPR–Cas9 genome editing.** The *GSX2*-mCherry hiPS cell reporter line was generated using a scarless genome editing method as previously described[58]. Briefly, guide RNA (gRNA)–Cas9 expression vectors were constructed by ligation of BbsI-digested px330-U6-Chimeric_BB-CBh-hSpCas9 (Addgene, plasmid 42230) with annealed oligonucleotides using T4 ligase (NEB). Editing design (position of homology arms, gRNA targets and primers for genotyping) and sequences of donor vectors are included in Extended Data Fig. 1 and Supplementary Tables 1 and 2. For gRNA design, no off-target candidates of any gRNAs used in this study were found by the COSMID tool[59] using the default search condition. Donor DNA plasmids were constructed using NEBuilder HiFi DNA Assembly (NEB, E2621S). The left and right homology arms for donor plasmids were amplified by nested PCR using genomic DNA extracted from K562 cells (ATCC, ATCC CCL-243), and other fragments were obtained by PCR amplification from previously reported vectors. hiPS cells ($2\times10^6$ cells) were electroporated using the P3 Primary Cell 4D-Nucleofector XL kit (V4XP-3024) and the 4D-Nucleofector system (Lonza, AAF-1002B) with 5 µg of the pX330 plasmid and 5 µg of donor plasmids, according to the manufacturer's protocol (program, CA-137). Cells were then cultured for 3 d in a well of a Matrigel-coated 6-well plate in mTeSR1 medium (Stemcell Technologies, 85850) supplemented with 10 µM Y27632 (Tocris, 1254) and then in mTeSR1 medium without Y27632. At 7 d post-nucleofection and following a 1 h pretreatment with 10 µM Y27632, cells were sorted twice using magnetic bead selection on MS and LD columns (Miltenyi Biotec, 130-042-201, 130-042-901) for first and second editing, respectively, and then transferred into columns with wash buffer (1% human albumin, 0.5 µM EDTA and 10 µM Y27632 in PBS). $CD8^+$ cells were selected with CD8 MicroBeads, which are magnetic beads conjugated with anti-human CD8 antibodies (Miltenyi Biotec, 130-045-201, 1:5 dilution). Seven days later, single hiPS colonies were picked based on GFP expression and genotyped by PCR with the following primers: FW (CTTCTATGTCGACTCGCTCATCATC) and RV (GGGCTGCTTTGAAAAAGTGAGATTA).

Image Lab software (version 5.2.1) was used for gel image acquisition.

**Generation of hStrSs and hCSs from hiPS cells.** For neural differentiation, hiPS cells were cultured on vitronectin-coated plates (5 µg ml$^{-1}$, Thermo Fisher Scientific, A14700) in Essential 8 medium (Thermo Fisher Scientific, A1517001). Cells were passaged every 4–5 d with UltraPure 0.5 mM EDTA, pH 8.0 (Thermo Fisher Scientific, 15575020). For the generation of 3D neural spheroids, hiPS cells were incubated with Accutase (Innovative Cell Technologies, AT104) at 37 °C for 7 min and dissociated into single cells. One to two days before spheroid formation, hiPS cells were exposed to 1% DMSO (Sigma-Aldrich, 472301) in Essential 8 medium. For aggregation into spheroids, approximately $3\times10^6$ single cells were added per well in AggreWell 800 plates in Essential 8 medium supplemented with the ROCK inhibitor Y27632 (10 µM, Selleck Chemicals, S1049), centrifuged at 100*g* for 3 min and then incubated at 37 °C with 5% $CO_2$. After 24 h, spheroids consisting of approximately 10,000 cells were collected from each microwell by pipetting medium up and down in the well with a cut P1000 pipette tip and transferred into ultra-low attachment plastic dishes (Corning, 3262) in Essential 6 medium (Thermo Fisher Scientific, A1516401) supplemented with the SMAD pathway inhibitors dorsomorphin (2.5 µM, Sigma-Aldrich, P5499) and SB-431542 (10 µM, R&D Systems, 1614). For the first 5 d, Essential 6 medium was changed every day and supplemented with dorsomorphin and SB-431542.

To generate hStrS, day 6 spheroids were transferred to neural medium containing Neurobasal-A medium (Thermo Fisher Scientific, 10888022), B-27 without vitamin A (Thermo Fisher Scientific, 12587010), GlutaMAX (1:100, Thermo Fisher Scientific, 35050079), penicillin–streptomycin (10,000 U ml$^{-1}$) (1:100, Thermo Fisher Scientific, 15140122), supplemented with the WNT pathway inhibitor IWP-2 (2.5 µM, Selleck Chemicals, S7085) and recombinant Human/Murine/Rat Activin A (50 µg ml$^{-1}$, PeproTech, 120-14P). On day 11, neural medium was supplemented with the retinoid X receptor agonist SR11237 (100 nM, Tocris, 3411), in addition to the compounds described above. From day 22, to promote differentiation of the neural progenitors into neurons, neural medium was supplemented with BDNF (20 ng ml$^{-1}$, PeproTech, 450-02), NT-3 (20 ng ml$^{-1}$, PeproTech, 450-03), AA (200 µM, Wako, 323-44822), $N^6$,2′-*O*-dibutyryladenosine-3′,5′ (cyclic)-monophosphate sodium salt (cAMP; 100 µM, MilliporeSigma, D0627) and DHA (10 µM, MilliporeSigma, D2534). From day 42, neural spheroids cultures were supplemented with DAPT (2.5 µM, Stemcell Technologies, 72082) in addition to BDNF, NT-3, AA, cAMP and DHA. From day 46, only neural medium containing B-27 Plus Supplement (Thermo Fisher Scientific, A3582801) was used for medium changes every 4 d.

hCSs were generated as previously described[12,57,60]. From day 22, the neural medium was supplemented with BDNF, NT-3, AA, cAMP and DHA. From day 46, only neural medium containing B-27 Plus Supplement was used for medium changes every 4 d.

**Dissociation of neural spheroids for 2D culture.** Three to four randomly selected hStrSs were collected in a 1.5-ml Eppendorf tube in a solution containing 10 U ml$^{-1}$ papain (Worthington Biochemical, LS003119), 1 mM EDTA, 10 mM HEPES (pH 7.4), 100 µg ml$^{-1}$ BSA, 5 mM L-cysteine and 500 µg ml$^{-1}$ DNase I (Roche, 10104159001). Cells were incubated at 37 °C for 15 min and gently shaken every 5 min. Papain was inactivated with FBS, and hStrSs were then gently triturated with a P1000 pipette. Samples were centrifuged twice at 1,300 rpm for 7 min, filtered with a 70-µm Flowmi Cell Strainer (Bel-Art, H13680-0070) and then suspended in neurobasal medium. Approximately $1\times10^5$ cells were seeded on 15-mm round coverslips (Warber Instruments, 64-0713) that were coated with approximately 0.001875% polyethylenimine (Sigma-Aldrich, 03880). Neurons were cultured in neural basal medium containing B-27 without vitamin A for 7 d (with half medium changes every other day). From day 7, cells were cultured in neurobasal medium containing B-27 Plus Supplement (with half medium changes every week). At days 65, 100 or 104, neurons were fixed in 4% paraformaldehyde (PFA), 4% sucrose dissolved in PBS for 20 min at 37 °C.

**Cryoprotection and immunocytochemistry.** hCSs, hStrSs, assembloids and E18.5 mouse brains were fixed in 4% PFA–PBS overnight at 4 °C. They were washed in PBS and transferred to 30% sucrose–PBS for 2–3 d until the 3D cultures or tissue sank in the solution. Subsequently, they were rinsed in optimal cutting temperature (OCT) compound (Tissue-Tek OCT Compound 4583, Sakura Finetek) and 30% sucrose–PBS (1:1) and embedded. For immunofluorescence staining, 10–18-µm-thick sections were cut using a Leica Cryostat (Leica, CM1850). Cryosections were washed with PBS to remove excess OCT and blocked in 10% normal donkey serum (NDS, MilliporeSigma, S30-M), 0.3% Triton X-100 (MilliporeSigma, T9284-100ML) and 1% BSA diluted in PBS for 1 h at room temperature. The sections were then incubated overnight at 4 °C with primary antibodies diluted in PBS containing 2% NDS and 0.1% Triton X-100. PBS was used to wash away excess primary antibodies, and the cryosections were incubated with secondary antibodies in PBS containing 2% NDS and 0.1% Triton X-100 for 1 h.

Dissociated cultures on glass coverslips were fixed in 4% PFA and 4% sucrose in PBS for 20 min at 37 °C and then rinsed twice for 5 min with PBS. hiPS cell cultures on glass coverslips were fixed in 4% PFA in PBS for 20 min at room temperature and rinsed twice with PBS for 5 min. Coverslips were blocked in 10% NDS, 0.3% Triton X-100, 1% BSA diluted in PBS for 1 h at room temperature and then incubated overnight at 4 °C with primary antibodies diluted in PBS containing 2% NDS and 0.1% Triton X-100. PBS was used to wash away excess primary antibodies, and the coverslips were incubated with secondary antibodies in PBS with 2% NDS and 0.1% Triton X-100. The following primary antibodies were used for staining: anti-calbindin (Synaptic Systems, 214 011, 1:200, 214011/5), anti-calretinin (rabbit, Swant, CR7697, 1:200), anti-MAP2 (guinea pig, Synaptic Systems, 188 004, 1:200 dilution, 2-26), anti-GFAP (rabbit, Dako, Z0334, 1:1,000 dilution, 20035993), anti-MBP (rat, Millipore, MAB386, 1:300 dilution), anti-ASCL1 (mouse, BD, 556604, 1:200 dilution, 6063825), anti-FOXP2 (mouse, Santa Cruz Biotechnology, sc-517261, 1:100 dilution, 1517), anti-GAD65 (goat, R&D Systems, AF2247, 1:100 dilution, UCX0218101), anti-CTIP2 (rat, Abcam, ab18465 1:300 dilution, GR322373-6, GR3272266-4), anti-DARPP32 (rabbit, Cell Signaling, 2306, 1:200 dilution, 7), anti-DARPP32 (rabbit, Abcam, ab40801, 1:200, GR3213231-3), anti-NeuN (mouse, Abcam, ab104224, 1:200, GR3341933-1), anti-GAD67 (mouse, MilliporeSigma, MAB5406, 1:200 dilution, 2676521), anti-GFP (chicken, GeneTex, GTX13970, 1:1,000 dilution, 821905323, 821704840, 821805508), anti-DRD2 (rabbit, MBL, MC-1405, 1:200, 107522), anti-mCherry (rabbit, GeneTex, GTX128508, 1:500 dilution, 42025), anti-PSD95 (guinea pig, Invitrogen, MA1-045, 1:200, SC249676), anti-SATB2 (mouse, Abcam, ab51502, 1:50 dilution, GR178264-4), anti-OCT4 (C30A3) (rabbit, Cell Signaling Technology, 2840, 1:200 dilution, 9), anti-SSEA4 (MC813) (mouse, Cell Signaling Technology, 4755, 1:200 dilution, 4). Alexa Fluor dyes, donkey anti-rabbit IgG (H&L) highly cross-adsorbed secondary antibody, Alexa Fluor 488 (Thermo Fisher Scientific, A-21206), donkey anti-mouse IgG (H&L) highly cross-adsorbed secondary antibody, Alexa Fluor 568 (Thermo Fisher Scientific, A10037, 2110843), donkey anti-rabbit IgG (H&L) highly cross-adsorbed secondary antibody, Alexa Fluor 568 (Thermo Fisher Scientific, A10042, 2136776), donkey anti-mouse IgG (H&L) highly cross-adsorbed secondary antibody, Alexa Fluor 647 (Thermo Fisher Scientific, A-31571, 1839633), donkey anti-goat IgG (H+L) highly cross-adsorbed secondary antibody, Alexa Fluor 647 (Thermo Fisher Scientific, A-21447, 1661244), Alexa Fluor 488 AffiniPure, donkey anti-chicken IgY (IgG) antibody (H&L) (Jackson ImmunoResearch, 703-545-155), Alexa Fluor 488 AffiniPure donkey anti-guinea pig IgG (H&L) antibody (Jackson ImmunoResearch, 706-545-148), Alexa Fluor 647

AffiniPure donkey anti-rat IgG (H&L) antibody (Jackson ImmunoResearch, 712-605-153), Alexa Fluor 647 AffiniPure donkey anti-rabbit IgG (H&L) antibody (Jackson ImmunoResearch, 711-605-152), Alexa Fluor 647 AffiniPure donkey anti-rat IgG (H&L) antibody (Jackson ImmunoResearch, 712-605-153) and Alexa Fluor 647 AffiniPure donkey anti-guinea pig IgG (H&L) (Jackson ImmunoResearch, 706-605-148) were used at a 1:1,000 dilution, and nuclei were visualized with Hoechst 33258 (Thermo Fisher Science, H3569, 1:10,000 dilution, 1829927). Cryosections and coverslips were mounted for microscopy on glass slides using Aquamount (Polysciences, 18606) and imaged on a Keyence BZ-X710, a Zeiss M1 Axioscope or a Leica TCS SP8 confocal microscope. Images were processed with Fiji (ImageJ, version 2.1.0, National Institute of Health (NIH)).

**Real-time qPCR.** mRNA from hCSs and hStrSs at days 15 and 22 was isolated using the RNeasy Mini kit (Qiagen, 74106) with DNase I, Amplification Grade (Thermo Fisher Scientific, 18068-015). Template cDNA was prepared by reverse transcription using the SuperScript III First-Strand Synthesis SuperMix for qRT–PCR (Thermo Fisher Scientific, 11752250). qPCR was performed using the SYBR Green PCR Master Mix (Thermo Fisher Scientific, 4312704) on a ViiA7 Real-Time PCR System (Thermo Fisher Scientific, 4453545). Primers used in this study are listed in Supplementary Table 4.

**Single-cell RNA-sequencing library preparation and data analysis.** To obtain a single-cell suspension, three to four hStrSs were randomly selected from each hiPS cell line at days 80 or 83 and collected in a 1.5-ml Eppendorf tube containing 10 U ml$^{-1}$ papain (Worthington Biochemical, LS003119) and 500 µg ml$^{-1}$ DNase I (Roche, 10104159001). The samples were then incubated in a 37 °C incubator for 15 min (with gentle shaking every 5 min). Papain was inactivated with 10% FBS in neurobasal medium, and hStrSs were gently triturated with a P1000 pipette. Samples were centrifuged at 1,300 rpm for 7 min, filtered with a 70-µm Flowmi Cell Strainer (Bel-Art, H13680-0070) and suspended in 0.04% BSA in PBS (MilliporeSigma, B6917-25MG) at a concentration of 1,000 cells per µl. Approximately 16,000 cells were loaded onto a Chromium Single Cell 3′ chip (Chromium Chip B Single Cell kit, 10x Genomics, PN-1000154) with the Chromium Single Cell 3′ Library & Gel Bead kit version 3 (10x Genomics, PN-1000075), and cDNA libraries were generated with the Chromium Single Cell 3′ Library Construction kit version 3 (10x Genomics, PN-1000078) according to the manufacturer's instructions. Each library was sequenced using the Illumina NovaSeq S4 2×150 bp by Admera Health. Quality control, UMI counting of Ensembl genes and aggregation of samples were performed by the 'count' and 'aggr' functions in Cell Ranger software (version 3.1.0). Further downstream analyses were performed using the R package Seurat (version 3.1.4)[61]. Genes on the X or Y chromosome were removed from the count matrix to avoid biases in clustering due to the sex of the hiPS cell line donors. Cells with more than 10,000 or less than 100 detected genes or with mitochondrial content higher than 15% were also excluded. Genes that were not expressed in at least three cells were not included in the analysis. Gene expression was normalized using a global-scaling normalization method (normalization method, 'LogNormalize'; scale factor, 10,000), and the 2,000 most variable genes were selected (selection method, 'vst') and scaled (mean = 0 and variance = 1 for each gene) before principal component analysis. The top 15 principal components were used for clustering (resolution of 0.5), using the 'FindNeighbors' and 'FindClusters' functions, and for visualization with UMAP. Clusters were grouped based on the expression of known marker genes and differentially expressed genes, as identified with the 'FindAllMarkers' function (Supplementary Table 6), and more resolved clusters and the top ten genes are shown in Extended Data Fig. 3d,e and Supplementary Table 7. Unbiased spatial mapping of the hStrS GABAergic neuron cluster was performed using VoxHunt[28]. Briefly, the 100 most variable features from the ISH Allen Brain Atlas data of the E13.5 mouse brain were selected, and similarity maps were calculated. These maps were then plotted in the sagittal and coronal views. Comparison of hStrS GABAergic neuron cluster data to BrainSpan transcriptomic data of microdissected human brain tissue was also performed using VoxHunt with default settings. Integration of hSS[19] (GSE93811, BD Resolve) and hStrS scRNA-seq datasets was performed using a standard Seurat version 3 integration workflow[62]. Before finding anchors between the individual datasets, the gene expression of two samples was normalized with the 'NormalizeData' function, and the 2,000 most variable genes were selected (selection method, 'vst') using the 'FindVariableFeatures' function. Anchors were identified using the 'FindIntegrationAnchors' function with a dimensionality of 5, and the standard workflows for visualization with UMAP and clustering were then used. Whether clusters were shared or not shared between hSSs and hStrSs was determined based on a bias for one of the conditions in the proportion of cells in each cluster. For instance, cluster 10 included 21.5% of all hSSs but only 1.07% of hStrSs; therefore, we considered this to be an hSS-biased cluster. On the other hand, an almost equal percentage of cells in both hSSs (5.38%) and hStrSs (6.04%) contributed to cluster 4; therefore, we considered this a shared cluster. The percentages for each condition can be seen in Extended Data Fig. 5c.

**Viral labeling and live-cell imaging.** Viral infection of 3D neural spheroids was performed as previously described[19,60]. Briefly, hCSs or hStrSs were transferred to a 1.5-ml Eppendorf tube containing 200 µl neural medium and incubated with virus overnight at 37 °C with 5% $CO_2$. The next day, fresh culture medium (800 µl) was added. The following day, neural spheroids were transferred into fresh culture medium in ultra-low attachment plates (Corning, 3471, 3261). For live-cell imaging, labeled hCSs, hStrSs or assembloids were transferred into one well of a Corning 96-well microplate (Corning, 4580) in 150 µl neural medium or onto a 20-mm glass coverslip in a 35-mm glass-bottom well (Cellvis, D35-20-0-N) and incubated in an environmentally controlled chamber for 15–30 min before imaging on a Leica TCS SP8 confocal microscope.

The viruses used were AAV-DJ-mDlx-GFP-Fishell-1 (ref. [33]) (Addgene, 83900), AAV-DJ-mDlx-GCaMP6f-Fishell-2 (ref. [33]) (Addgene, 83899), AAV-DJ-hSyn1::eYFP (Stanford University Neuroscience Gene Vector and Virus Core, GVVC-AAV-16), AAV-DJ-CaMKIIa::eYFP (Stanford University Neuroscience Gene Vector and Virus Core, GVVC-AAV-8), AAV-DJ-hSyn1::mCherry (Stanford University Neuroscience Gene Vector and Virus Core, GVVC-AAV-17), rabies-ΔG-Cre-eGFP (Salk Institute Viral Vector Core), AAV-DJ-EF1a-CVS-G-WPRE-pGHpA[63] (Addgene, 67528), AAV-DJ-EF1-DIO-mCherry (Stanford University Neuroscience Gene Vector and Virus Core, GVVC-AAV-14), AAV1-Syn::ChrimsonR-tdT[43] (Addgene, 59171-AAV1), AAV-DJ-Ple94 (GPR88)-iCre[35] (pEMS1995, Addgene, 49125), AAV-DJ-EF1-DIO-eYFP (Stanford University Neuroscience Gene Vector and Virus Core, GVVC-AAV-13), AAV-DJ-EF1a-DIO-GCaMP6s (Stanford University Neuroscience Gene Vector and Virus Core, GVVC-AAV-91).

For imaging and quantification of dendritic spines in hStrSs, mDLX::eGFP$^+$ cells were imaged using ×10 and ×20 objectives on a Leica TCS SP8 confocal microscope, and images were analyzed with Fiji (ImageJ, version 2.1.0, NIH). The number of dendritic spines on a primary and a secondary dendrite within 200 µm of the soma were counted.

For calcium imaging, hStrSs or assembloids were labeled with AAV-DJ-Ple94::iCre and AAV-DJ-EF1a::DIO-GCaMP6s or mDLX::GCaMP6f-Fishell-2 and placed in a well of a Corning 96-well microplate (Corning, 4580) or on a 20-mm coverslip glass in a 35-mm glass-bottom plate in neural medium and imaged using a ×10 objective on a Leica TCS SP8 confocal microscope. GCaMP6 was imaged at a frame rate of 14.7 frames per second, and results were analyzed with Fiji (ImageJ, version 2.1.0, NIH) and MATLAB (version R2018a, 9.4.0, MathWorks).

**Generation of cortico-striatal assembloids.** To generate cortico-striatal assembloids, hCSs and hStrSs were derived separately and fused by placing them in close proximity in 1.5-ml Eppendorf tubes for 3 d in an incubator. The medium was carefully changed on day 2, and, on day 3, assembloids were placed in 6-well or 60-mm ultra-low attachment plates (Corning, 3471, 3261) in neural medium as described. Assembly was performed between days 60 and 76 of differentiation.

**Clearing and 3D staining of cortico-striatal assembloids.** To optically clear cortico-striatal assembloids, we applied the hydrophilic chemical cocktail-based CUBIC protocol[64,65]. Briefly, cortico-striatal assembloids at day 83 were fixed with a 4% PFA–4% sucrose–PBS solution at 37 °C for 20 min and incubated at 4 °C overnight. The next day, assembloids were washed twice with PBS and incubated in Tissue-Clearing Reagent CUBIC-L (TCI, T3740) at 37 °C for 2 d. Assembloids were washed three times with PBS for 2 h and then stained with anti-GFP (1:1,000 dilution) and anti-mCherry (1:1,000 dilution) antibodies in PBS containing 0.2% Triton X-100 and 3% NDS at 37 °C for 2 d. Assembloids were subsequently washed three times with PBS for 2 h and then incubated with secondary antibodies (Alexa Fluor, 1:1,000 dilution) in PBS containing 0.2% Triton X-100 and 3% NDS at 37 °C for 2 d. For refractive index matching, assembloids were incubated with Tissue-Clearing Reagent CUBIC-R+ (TCI, T3741) at room temperature for 2 d. CUBIC-cleared assembloids were then transferred into a well of a Corning 96-well microplate (Corning, 4580) in 150 µl of CUBIC-R+ solution and imaged using a ×10 objective on a Leica TCS SP8 confocal microscope.

**Axon projection imaging in cortico-striatal assembloids.** AAV-DJ-hSyn1::eYFP$^+$ cells projecting into hStrSs from hCSs or AAV-DJ-hSyn1::mCherry$^+$ cells projecting into hCSs from hStrSs were imaged under environmentally controlled conditions in cortico-striatal assembloids using the Leica TCS SP8 confocal microscope with a motorized stage. Assembloids were transferred to a well in a Corning 96-well microplate (Corning, 4580) in 150 µl culture medium and incubated in an environmentally controlled chamber for 15–30 min before imaging. Images were taken using a ×10 objective lens at a depth of 0–500 µm. The percentage of eYFP coverage in hStrSs and of mCherry coverage in hCSs were quantified with Fiji (ImageJ, version 2.1.0, NIH).

**Retrograde rabies tracing in cortico-striatal assembloids.** For retrograde neural tracing experiments in cortico-striatal assembloids, hCSs were labeled with AAV-DJ-EF1-DIO-mCherry and hStrSs were labeled with rabies-ΔG-Cre-eGFP and AAV-DJ-EF1a-CVS-G-WPRE-pGHpA. After viral infection, hCSs and hStrSs were assembled and maintained in culture with medium changes every 4 d. At 28 d after assembly, cortico-striatal assembloids were fixed overnight in 4% PFA in PBS at 4 °C and processed for immunostaining. Images were taken with a Leica TCS SP8 confocal microscope and analyzed in Fiji (ImageJ, version 2.1.0, NIH).

**Optogenetic stimulation and calcium imaging.** Cortico-striatal assembloids expressing AAV1-Syn::ChrimsonR-tdTomato in hCSs or AAV-DJ-Ple94-iCre and

AAV-DJ-EF1a::DIO-GCaMP6s in hStrSs were placed on a 20-mm coverslip glass in a 35-mm glass-bottom plate in neural medium and imaged using a ×10 objective on a Leica TCS SP8 confocal microscope. For optogenetic stimulation, ChrimsonR–tdTomato$^+$ cells in hCSs were activated with 625-nm light using an optical fiber-coupled LED (400-µm diameter, 13.2 mW, Thorlabs). GCaMP6s was imaged at a frame rate of 14.7 frames per second. Stimulation experiments included 1,500 frames, and one 625-nm pulse of LED light (68 ms) was applied every 150 frames or 300 frames. The pulse was generated by a Cyclops LED connected to the Leica TCS SP8 microscope. Results were analyzed with Fiji (ImageJ, version 2.1.0, NIH) and MATLAB (version R2018a, 9.4.0, MathWorks). After registration of regions of interest, raw time series were transformed to relative changes in fluorescence as follows: $\Delta F/F_t = (F_t - F_0)/F_0$. To verify whether responses were time-locked to the LED stimulation, $\Delta F/F$ responses were compared to $\Delta F/F$ values at randomly selected time points. For time-locked $\Delta F/F$ values, the amplitudes of $\Delta F/F$ values from each cell were calculated as the maximum $\Delta F/F$ value within a 20–30-frame (1,360–2,040 ms) window following LED stimulation (minus the mean of the baseline 1 s before stimulation). The median was used to exclude shape-dependent artifacts; the median amplitude of $\Delta F/F$ values was compared before and after treatment with the AMPA receptor antagonist NBQX (20 µM, Tocris, 0373), the NMDA receptor antagonist D-APV (50 µM, Tocris, 0106) and the $GABA_A$ receptor antagonist (+)-bicuculline (50 µM, Tocris, 0130). To analyze synchronization of calcium signals, mean correlation coefficients per pair of cells of $\Delta F/F$ values from GCaMP6 signals in hStrSs and cortico-striatal assembloids were analyzed in MATLAB.

**Whole-cell recordings.** Whole-cell recordings in neural spheroid slices were performed as previously described[19,57]. Briefly, assembloid or spheroid slices were embedded in 4% agarose and transferred to an artificial cerebrospinal fluid (aCSF) containing 126 mM NaCl, 2.5 mM KCl, 1.25 mM $NaH_2PO_4$, 1 mM $MgSO_4$, 2 mM $CaCl_2$, 26 mM $NaHCO_3$ and 10 mM D-(+)-glucose. Slices were cut at 200 µm at room temperature using a Leica VT1200 vibratome and maintained in aCSF at room temperature.

Whole-cell patch-clamp recordings from hStrS slices were performed under an upright SliceScope microscope (Scientifica). Slices were perfused with aCSF (bubbled with 95% $O_2$ and 5% $CO_2$), and signals from cells were recorded at 30 °C. hSyn1::eYFP$^+$ neurons were patched with a borosilicate glass pipette filled with an internal solution containing 127 mM potassium gluconate, 8 mM NaCl, 4 mM magnesium ATP, 0.3 mM sodium GTP, 10 mM HEPES and 0.6 mM EGTA, pH 7.2, adjusted with KOH (290 mOsm). Data were acquired with a MultiClamp 700B Amplifier (Molecular Devices) and a Digidata 1550B Digitizer (Molecular Devices), low-pass filtered at 2 kHz, digitized at 20 kHz and analyzed with pCLAMP software (version 10.6, Molecular Devices). The liquid junction potential was calculated using JPCalc[66], and recordings were corrected with an estimated −15-mV liquid junction potential[67–69].

sEPSCs were recorded at −70 mV in voltage-clamp mode and analyzed with Mini Analysis software (version 6.0.3, Synaptosoft). For *F–I* curves, cells were current-clamped at −60 mV; current steps (1-s duration) were given with an increment of 10 pA. Data were analyzed with in-house programs in MATLAB (MathWorks). For LED stimulation, 5-ms-long whole-field illumination at 550 nm (maximal power, CoolLed) was applied through the ×40 objective, and oEPSCs were recorded at −70 mV. AAV-hSyn1::eYFP$^+$ neurons close to the hCS side of cortico-striatal assembloids were randomly selected for recordings.

**Animals.** Pregnant ICR/CD1 mice were obtained from Charles River. Whole brains from E18.5 mouse embryos were fixed with cold 4% PFA–PBS, and samples were prepared following the staining method described above. Approval for mouse experiments was obtained from the Stanford University Administrative Panel on Laboratory Animal Care (APLAC).

**Statistics.** Data are presented as mean ± s.e.m. or box plots showing maximum, third quartile, median, first quartile and minimum values. Raw data were tested for normality of distribution, and statistical analyses were performed using paired or unpaired *t*-tests (two-tailed), Mann–Whitney tests, Kruskal–Wallis tests, Wilcoxon tests or one-way ANOVA tests with multiple comparison and two-way ANOVA tests. Sample sizes were estimated empirically. GraphPad Prism version 8.4.2 was used for statistical analyses.

**Reporting Summary.** Further information on research design is available in the Nature Research Reporting Summary linked to this article.

## Data availability

Gene expression data were deposited in the Gene Expression Omnibus under accession number GSE149931. The Human Brain Transcriptome (https://hbatlas.org/) was used to explore transcriptomic data of the developing and adult human brain[27].The data in this study are available on request from the corresponding author. Source data are provided with this paper.

## Code availability

The codes used for calcium imaging and electrophysiology analyses in this study are available on request from the corresponding author.

## References


57. Yoon, S. J. et al. Reliability of human cortical organoid generation. *Nat. Methods* **16**, 75–78 (2019).
58. Ikeda, K. et al. Efficient scarless genome editing in human pluripotent stem cells. *Nat. Methods* **15**, 1045–1047 (2018).
59. Cradick, T. J., Qiu, P., Lee, C. M., Fine, E. J. & Bao, G. COSMID: a web-based tool for identifying and validating CRISPR/Cas off-target sites. *Mol. Ther. Nucleic Acids* **3**, e214 (2014).
60. Sloan, S. A., Andersen, J., Pasca, A. M., Birey, F. & Pasca, S. P. Generation and assembly of human brain region-specific three-dimensional cultures. *Nat. Protoc.* **13**, 2062–2085 (2018).
61. Butler, A., Hoffman, P., Smibert, P., Papalexi, E. & Satija, R. Integrating single-cell transcriptomic data across different conditions, technologies, and species. *Nat. Biotechnol.* **36**, 411–420 (2018).
62. Stuart, T. et al. Comprehensive integration of single-cell data. *Cell* **177**, 1888–1902 (2019).
63. Wertz, A. et al. Single-cell-initiated monosynaptic tracing reveals layer-specific cortical network modules. *Science* **349**, 70–74 (2015).
64. Susaki, E. A. et al. Whole-brain imaging with single-cell resolution using chemical cocktails and computational analysis. *Cell* **157**, 726–739 (2014).
65. Tainaka, K. et al. Chemical landscape for tissue clearing based on hydrophilic reagents. *Cell Rep.* **24**, 2196–2210 (2018).
66. Barry, P. H. JPCalc, a software package for calculating liquid junction potential corrections in patch-clamp, intracellular, epithelial and bilayer measurements and for correcting junction potential measurements. *J. Neurosci. Methods* **51**, 107–116 (1994).
67. Paz, J. T. et al. Closed-loop optogenetic control of thalamus as a tool for interrupting seizures after cortical injury. *Nat. Neurosci.* **16**, 64–70 (2013).
68. Sorokin, J. M. et al. Bidirectional control of generalized epilepsy networks via rapid real-time switching of firing mode. *Neuron* **93**, 194–210 (2017).
69. Makinson, C. D. et al. Regulation of thalamic and cortical network synchrony by Scn8a. *Neuron* **93**, 1165–1179 (2017).


## Acknowledgements


We thank members of the Pasca laboratory at Stanford University for scientific input and the Stanford Wu Tsai Neurosciences Institute Virus Core for production of AAVs. This work was supported by a US NIH BRAINS Award (MH107800) (to S.P.P.), an MQ Fellow Award (to S.P.P.), an NYSCF Robertson Stem Cell Investigator Award (to S.P.P.), the Stanford Human Brain Organogenesis Program in the Wu Tsai Neurosciences Institute (to S.P.P.), the Kwan Research Fund (to S.P.P.), the Coates Foundation (to S.P.P.), the Senkut Foundation (to S.P.P.), the Uytengsu Research Fund (to S.P.P.), the Chan Zuckerberg Initiative Ben Barres Investigator Award (to S.P.P.), the Stanford Medicine Dean's Fellowship (to Y.M. and F.B.), the Stanford Maternal & Child Health Research Institute (MCHRI) Postdoctoral Fellowship (to Y.M., F.B. and O.R.) and the American Epilepsy Society Postdoctoral Research Fellowship (to F.B.).


## Author contributions

Y.M., F.B. and S.P.P. conceived the project and designed experiments. Y.M. and F.B. performed differentiation experiments and characterized spheroids. Y.M. carried out scRNA-seq experiments and related analyses and performed functional imaging assays. M.-Y.L. conducted and analyzed the electrophysiological characterization. K.I. and M.H.P. generated and validated the *GSX2*-mCherry hiPS cell line. O.R. developed MATLAB codes for calcium imaging, analyzed the results and prepared the mouse brain samples. M.V.T. performed differentiation experiments and characterized spheroids. J.-Y.P. contributed to the characterization of spheroids and the quantification of retrograde tracing. A.P. contributed to differentiation experiments. S.H.L. contributed to the characterization of spheroids from 22q13.3DS and control hiPS cell lines. Y.M. and S.P.P. wrote the manuscript with input from all authors.

## Competing interests

Stanford University has filed a provisional patent application covering the protocol and methods for the generation of human striatal organoids and cortico-striatal assembloids. M.H.P. is a consultant for and has equity interest in CRISPR Tx. Throughout the duration of this study, K.I. was an employee of Daiichi Sankyo Co., Ltd, although the company had no input in the design or execution of the study or the interpretation or publication of data.

## Additional information

**Extended data** is available for this paper at https://doi.org/10.1038/s41587-020-00763-w.

**Supplementary information** is available for this paper at https://doi.org/10.1038/s41587-020-00763-w.

**Correspondence and requests for materials** should be addressed to S.P.P.

**Peer review information** *Nature Biotechnology* thanks Zhanyan Fu, Guoping Feng and the other, anonymous, reviewer(s) for their contribution to the peer review of this work.

**Reprints and permissions information** is available at www.nature.com/reprints.